

DEVELOPMENT OF THGEM BASED DETECTORS FOR AT-TPC APPLICATIONS

By

Stefan Hermann Rost

A THESIS

Submitted to
Michigan State University
in partial fulfillment of the requirements
for the degree of

Physics - Master of Science

2016

ABSTRACT

DEVELOPMENT OF THGEM BASED DETECTORS FOR AT-TPC APPLICATIONS

By

Stefan Hermann Rost

Studying unstable nuclei away from the line of stability using low energy reactions is of high interest in modern nuclear physics. The low energy ions observed in these reactions lose most of their energy within the target, therefore the construction of an Active Target Time Projection Chamber (AT-TPC), detecting the track within the target, is an attractive solution. In order to maximize the reaction yield while minimizing background operation in pure gas without quench gas is necessary. In pure gas, however, the transition to streamer mode (discharge) occurs already at low gain when using common structures (e.g. GEM (gas electron multiplier)), therefore a new type of detector functioning at high gain in pure elemental gas is required. Two THick Gaseous Electron Multipliers (THGEM) in cascade were found to operate at a gain of up to 10^4 in pure helium for pressures between 200 torr and 600 torr, while also providing a good energy resolution. The THGEM is a hole-type gaseous electron multiplier produced by multi layer printed circuit board (PCB) technology. It consists of a densely perforated assembly of 0.6 mm thick FR-4 substrate, sandwiched between thin metallic electrode strata. Three THGEMs were stacked together to form a novel gaseous multiplier (M-THGEM), providing a high confinement of the electron avalanche within the hole, resulting in a gain of up to $10^{4.5}$ in pure low-pressure helium. It demonstrated a very good energy resolution in the experiment and an estimated ion backflow of as low as 13% in simulations. Furthermore, it is extremely suitable to cover large areas due to its robustness, making the three layer M-THGEM suitable for a large detector such as the AT-TPC.

ACKNOWLEDGMENTS

I would like to thank my advisor, Prof. Daniel Bazin, for his unwavering support during my work at the National Superconducting Laboratory. When I needed help, his door was always open.

This project would not have been possible without Marco Cortesi. He introduced me to the research field of gaseous detector development, acting as my mentor and teacher during my time in the laboratory. His patient explanations guided me through many obstacles along the way.

Prof. Wolfgang Mittig's knowledgeable input was a valuable resource throughout the research.

My sincere thanks also go to my group, for the fruitful discussions on difficulties and results. The support of the mechanical and electronic engineers was critical to the development of the experiment.

TABLE OF CONTENTS

LIST OF TABLES	vi
LIST OF FIGURES	vii
KEY TO SYMBOLS	xii
KEY TO ABBREVIATIONS	xiii
Chapter 1 Introduction	1
Chapter 2 Operating principles of gaseous detectors	3
2.1 Avalanche process	3
2.1.1 Gain	3
2.1.1.1 Long term gain stability	4
2.1.1.2 Penning effect	5
2.1.1.3 Impurities	5
2.1.2 Ion feedback	6
2.1.3 Photon feedback	6
2.1.4 Limit of gain	7
2.2 Hole-type detector structures	8
2.2.1 Two cascade THGEMs	9
2.2.2 Three-layer M-THGEM	10
2.3 Signal formation	11
Chapter 3 Simulations	13
3.1 Field simulation	13
3.1.1 Two cascade THGEMs	13
3.1.2 Three-layer M-THGEM	15
3.1.2.1 Symmetric voltages	15
3.1.2.2 Asymmetric voltages	16
3.2 Particle drift	16
3.2.1 Range in the AT-TPC	16
3.2.1.1 SRIM (energy loss calculation)	16
3.2.1.2 MCNPX (alternate energy loss calculation)	17
3.2.2 Electron collection efficiency	19
3.2.3 Gain	20
3.2.3.1 Different geometries and gases	20
3.2.3.2 Two cascade THGEMs	21
3.2.3.3 Three-layer M-THGEM	24
3.2.4 Ion backflow	27

3.2.4.1	Transfer field and ion feedback	27
3.2.4.2	Influence of the relative alignment between the two THGEMs on electron and ion transfer	29
3.2.4.3	Collection of Ions in the three-layer M-THGEM	30
3.2.4.4	Ionfeedback vs. Gain for different configurations	34
Chapter 4	Measurements for the two cascade THGEMs	36
4.1	Experimental Setup	36
4.1.1	Gas handling system	36
4.1.2	Voltage power supplies	37
4.1.3	Readout electronics	37
4.2	Performance in Helium	38
4.2.1	Gain	38
4.2.2	Energy resolution	39
4.3	Performance in Hydrogen	40
4.3.1	Gain	40
4.3.2	Electron drift velocity	41
4.4	Further interpretation of measurements	42
Chapter 5	Towards a new generation of M-THGEMs: Three-layer M- THGEM	44
Chapter 6	Conclusion and outlook	48
APPENDICES	50
	Appendix A Additional graphs	51
	Appendix B Technical advice	53
	Appendix C Manual for performing simulations of THGEMs within the NSCL . .	54
BIBLIOGRAPHY	76

LIST OF TABLES

Table 3.1:	Range of alpha particles in helium simulated using SRIM	17
Table 3.2:	Range of alpha particles in hydrogen simulated using MCNPX. . . .	19
Table 4.1:	Drift velocity of electrons in hydrogen according to Fig. 4.5.	41
Table 4.2:	$\frac{\gamma}{p}$ calculated from the linear fits for the curves in Fig. 4.6.	43

LIST OF FIGURES

Figure 1.1:	Visualization of the AT-TPC working principle. Figure taken from [1]	1
Figure 2.1:	Illustration of one single avalanche.	4
Figure 2.2:	Visualization of the secondary emission from the electrode due to photons. Figure taken from [9].	6
Figure 2.3:	Illustration of the formation of streamers and the resulting area of ionized gas (left to right). Inspired by Ref. [13]	8
Figure 2.4:	Schematic drawing of a two cascade THGEM setup, like it is used in the AT-TPC.	9
Figure 2.5:	Setup of two cascade THGEMs including the micromegas. The image is created in Garfield [5] and shows the drift lines of electrons in vacuum.	10
Figure 2.6:	Setup of the three layer M-THGEM including the visualization of an avalanche created by a single electron. The image is made using Garfield [5].	11
Figure 3.1:	Simulation of the electrical dipole field on top of a THGEM (left). Plot of the electrical field magnitudes within the whole structure of two cascade THGEMs. The drift field is set to $0.5 \frac{\text{kV}}{\text{cm}}$, the induction field is set to $1.5 \frac{\text{kV}}{\text{cm}}$ and the transfer field is $1.5 \frac{\text{kV}}{\text{cm}}$. The voltage across one THGEM is 1500 V.	14
Figure 3.2:	Simulation of the electric field strength within a three layer M-THGEM (left). The voltage across all layers of the M-THGEM is the same. Plot of the electric field strength along a vertical cut through the plot on the left, showing the field enhancement in the center of the M-THGEM (right).	15
Figure 3.3:	Simulation of the field strength within a three layer M-THGEM. On the left, the voltage applied to all layers is equivalent, on the right the top layer is reduced to 3 (70%).	16
Figure 3.4:	Range within the AT-TPC using pure Helium at 400 torr. The energy loss per angstrom is plotted as function of the penetration depth. The $3.6 \mu\text{m}$ thick para-aramid window is taken into account.	17

Figure 3.5:	Range within the AT-TPC using pure Hydrogen at 400 torr. The resulting energy distribution is shown in Fig. 3.6.	18
Figure 3.6:	Distribution of the eneregy deposition in hydrogen within the AT-TPC, taking into account the window and angle distribution of the source.	18
Figure 3.7:	Collection efficiency for a three-layer M-THGEM in pure helium at 200 torr. The percentages given describe the potential difference in the first layer compared to the other layers for different asymmetric voltage configuration.	20
Figure 3.8:	Gain curves for all different geometries discussed in this work. The data is generated using garfield [5] at a pressure of 600 torr for all curves.	21
Figure 3.9:	Gain curves for different pressures in pure helium, using a transfer field of $0.25 \frac{\text{kV}}{\text{cm}}$ and an induction field and drift field of $0.5 \frac{\text{kV}}{\text{cm}}$	22
Figure 3.10:	Gain curves for different pressures in pure hydrogen, using a transfer field of $0.25 \frac{\text{kV}}{\text{cm}}$ and an induction field and drift field of $0.5 \frac{\text{kV}}{\text{cm}}$	23
Figure 3.11:	Gain curves for different pressures in pure helium, using an induction field and drift field of $0.5 \frac{\text{kV}}{\text{cm}}$	25
Figure 3.12:	Gain curves for different pressures in pure hydrogen, using an induction field of $1.5 \frac{\text{kV}}{\text{cm}}$ and drift field of $0.1 \frac{\text{kV}}{\text{cm}}$. The graph includes gains for the two different operation modes, symmetric voltages and asymmetric voltages (first THGEM 70%).	26
Figure 3.13:	Plot of the ion tracks (red) and electron tracks (orange) in one avalanche for a setup with two cascade THGEMs. The plots are generated in H_2 at 400 torr with a voltage of 1025 V across each THGEM using garfield [5]. The potential differences are: drift field $0.1 \frac{\text{kV}}{\text{cm}}$, induction field $1.5 \frac{\text{kV}}{\text{cm}}$, transferfield $1.5 \frac{\text{kV}}{\text{cm}}$ (left) and $0.125 \frac{\text{kV}}{\text{cm}}$ (right).	27
Figure 3.14:	Corresponding to Fig. 3.13 the histograms on the left show the end-points for ions and electrons using a high transfer field, whereas on the right these values are shown for a weak transfer field.	28

Figure 3.15:	Plot of the ion tracks (red) and electron tracks (orange) in one avalanche for two cascade THGEMs, which are not aligned. The plots are generated in H ₂ at 400 torr with a voltage of 1050 V across each THGEM using garfield [5]. The drift field is set to $0.1 \frac{\text{kV}}{\text{cm}}$, the transferfield is set to $0.125 \frac{\text{kV}}{\text{cm}}$ and the induction field is $1.5 \frac{\text{kV}}{\text{cm}}$. The left picture shows a 3D view and the right diagram a 2D illustration.	30
Figure 3.16:	Statistics of the endpoints for ions (right) and electrons (left) in the two cascade THGEMs, which are not aligned like shown in Fig. 3.15. The plots are generated in H ₂ at 400 torr with a voltage of 1050 V across each THGEM using garfield [5]. The drift field is set to $0.1 \frac{\text{kV}}{\text{cm}}$, the transferfield is set to $0.125 \frac{\text{kV}}{\text{cm}}$ and the induction field is $1.5 \frac{\text{kV}}{\text{cm}}$. .	31
Figure 3.17:	Plot of the ion tracks (red) and electron tracks (orange) in one avalanche for a three-layer M-THGEM. The plots are generated in H ₂ at 400 torr with a voltage of 650 V across each THGEM using garfield [5]. The drift field is set to $0.1 \frac{\text{kV}}{\text{cm}}$ and the induction field is $1.5 \frac{\text{kV}}{\text{cm}}$. The left picture shows a 3D view and the right diagram a 2D illustration. . .	32
Figure 3.18:	Corresponding to Fig. 3.17 the histograms on the left show the endpoints for ions and electrons using a high symmetric voltage of 650 V for each THGEM, whereas on the right the first THGEM is working as a collector (asymmetric voltage configuration). It is set to 70% of the full voltage.	33
Figure 3.19:	Ion backflow (number of ions at the cathode over number electrons at the anode) plotted against the gain for a three-layer M-THGEM and two cascade single layer THGEMs in H ₂ at 400 torr. The decrease in IBF for higher gain is clearly visible for each setup. The error is indicated as the $\sigma/2$ spread of the simulation.	34
Figure 4.1:	Calibration curves for the charge amplifier for the two different amplifications. The slope of the two curves are $6 \frac{\text{electrons}}{\text{bin}}$ and $60 \frac{\text{electrons}}{\text{bin}}$ respectively.	37
Figure 4.2:	Comparison of the gain in pure helium for different pressures. The horizontal lines indicate the maximum achievable gain. In addition three measurements by Marco Cortesi [9] using UV-Light are included. .	38
Figure 4.3:	Visualization for 2000 events in helium at 600 torr (left). The energy spectrum calculated from these events (right).	39

Figure 4.4:	Comparison of the gain in pure hydrogen for different pressures. The endpoint of each curve indicates the maximum achievable gain at that pressure.	40
Figure 4.5:	Visualization of 1000 events in hydrogen for different pressures. . . .	41
Figure 4.6:	Comparison of the gain in pure hydrogen for different pressures. The curves in this graph are used to fit the parameter $\frac{\gamma}{p}$	42
Figure 5.1:	A schematic drawing (left (topview) and top right (sideview)) and a photograph (bottom right) of the mounted M-THGEM.	44
Figure 5.2:	Spectrum of a 5.5 MeV alpha particle crossing the pAT-TPC active volume, recorded with the three layer M-THGEM operated in He-based mixture (10% CO ₂).	45
Figure 5.3:	Gain measurement for the three layer M-THGEM (schematic drawing(a)) in He/(10%)CO ₂ (b) and in pure He (c).	46
Figure 5.4:	Comparison of the electric field map for a three layer M-THGEM hole symmetrically biased (a) and asymmetric biased (b). β represents the reduced fraction of the applied potential to the first multiplier stage. Measurements of effective gain in 200 torr He/10%CO ₂ for different three layer M-THGEM configurations.	47
Figure 5.5:	Comparison of the electron collection efficiency (a) and ion backflow (b) in He/10%CO ₂ for different asymmetric M-THGEM configurations.	47
Figure A.1:	Comparison between the experimental data (Fig. 4.2) in helium for the two cascade THGEMs and the simulated results (Fig. 3.9). The significant discrepancy can be explained by the missing Penning effect in garfield [5].	51
Figure A.2:	Comparison between the experimental data (Fig. 4.4) in hydrogen for the two cascade THGEMs and the simulated results (Fig. 3.10). The significant discrepancy can be explained by residue oxygen, capturing free electrons.	52
Figure C.1:	“record script” function in Maxwell	56
Figure C.2:	Start Mobaxterm and enter host name.	59
Figure C.3:	Correct settings in notepad++, to modify the file for submitting to the batch system. The correct line ending “LF” is shown.	70

Figure C.4: Wrong (windows) line break in the file for submitting to the batch system.	71
--	----

KEY TO SYMBOLS

- E_{trans} - Electric transfer field
- E_{drift} - Electric drift field
- E_{ind} - Electric induction field
- V - Voltage
- ΔV - Voltage difference across one THGEM
- Φ - Electrical field
- I - current
- q - charge
- E^W - weighting field
- G - Gain
- α - Townsend coefficient
- γ - electron mean free path

KEY TO ABBREVIATIONS

- AT-TPC - Active Target Time Projection Chamber
- GEM - Gaseous Electron Multipliers
- THGEM - THick Gaseous Electron Multipliers
- M-THGEM - Multilayer THGEM
- FWHM - Full Width Half Maximum
- IBF - Ion Backflow

Chapter 1

Introduction

Studying the structural evolution and the reaction dynamics of unstable nuclei away from the line of stability is of high interest in modern nuclear physics [1]. Modern accelerator facilities (e.g. NSCL [2]) provide radioactive beams over a wide domain of the nuclear chart. When these heavy-ion beams collide with a light-ion target, most of the reaction energy is carried away by the heavy ions. In detecting the light ions with low recoil energy of 0.1-10 MeV [1], a large portion of their kinetic energy is lost within the target, therefore conventional detectors (HiRA [3], HELIOS [4]) can only detect part of the kinetic energy, often resulting in a poor energy resolution.

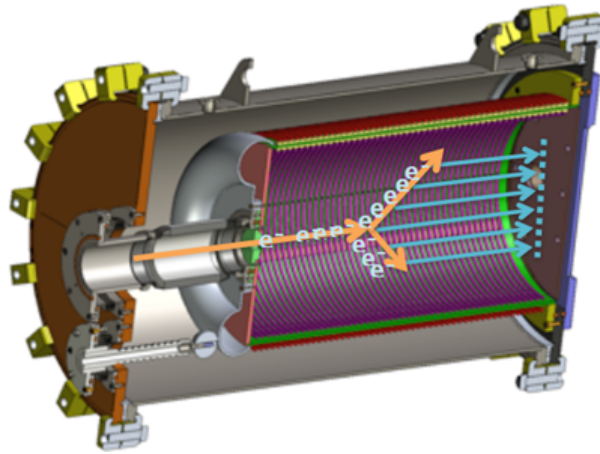


Figure 1.1: Visualization of the AT-TPC working principle. Figure taken from [1]

The construction of a detector for which tracking of particles is possible within the target can circumvent this issue. Active Target Time Projection Chambers (AT-TPC) are gaseous detectors in which a large volume of a low-mass filling gas acts simultaneously as ionization

medium and target. The electrons created by a particle travelling through the volume are detected with spatial resolution at the end of the chamber (Fig. 1.1). Combining this data with timing information, the track of a particle in the active volume can be reconstructed in 3D [1]. An AT-TPC requires an electron multiplier capable of delivering a large dynamic range and high gain in low-pressure operation in pure elemental gas (H_2 , D_2 , ^3He , ^4He , etc.). The operation without a quencher is important because it maximizes the reaction yield with minimal background subtraction. Without the use of a quench gas only reactions with the desired target atoms occur, for example when using a proton target only reactions with H_2 are visible, instead of having additional collisions with a quench gas like CO_2 . It is difficult to reach stable high-gain operation of proportional gaseous detectors under these conditions (low pressure and no quencher), mainly due to the considerable photon-mediated secondary effects that lead to an early transition from proportional avalanche mode to streamer mode (discharge). THGEMs, especially in a cascade setup or as multilayer THGEM (M-THGEM), can solve these issues. THGEMs are a hole type structure of 0.5 mm - 1 mm thickness, consisting of two copper layers separated by an isolator. A voltage is applied across the gap between the two electrodes. Through avalanche processes electrons are multiplied in this gap.

It is essential to determine the energy resolution and the gain, depending on the voltage difference ΔV . This investigation is the subject of the present work through experimental data and simulations performed in Garfield [5]. It is followed by the investigation of an innovative new THGEM concept: a multilayer THGEM (M-THGEM) that consists of multiple THGEMs combined into one module, significantly improving the performance.

Chapter 2

Operating principles of gaseous detectors

2.1 Avalanche process

2.1.1 Gain

Gain, amplification (multiplication) of a incoming electron signal, in a gaseous multiplier is achieved via the creation of new electron-ion pairs. A new electron-ion pair is created when the energy transferred from a collision is greater than the ionization energy of the gas atom or molecule. Once the electron has gained enough energy from the electric field (by acceleration), a new electron-ion pair can be created. This process creates an avalanche of electrons if the drift length in the multiplication area is long enough (Fig. 2.1). During the acceleration process of a electron, elastic and inelastic collisions with gas atoms or molecules occur. The excited gas atoms, can emit a photon causing secondary effects described in section 2.1.3 and 2.1.4. The frequency of collisions depends on the electrons mean free path, which increases when the gas pressure is decreased.

Multiplication in a gas can be described using the first Townsend coefficient (α)

$$G = e^{\alpha d},$$

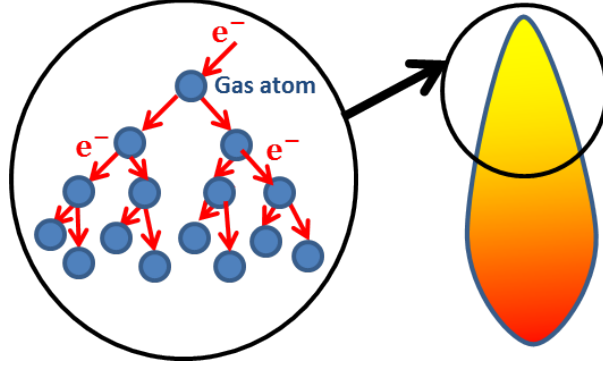


Figure 2.1: Illustration of one single avalanche.

with d being the length of the multiplication zone. At high reduced electric field strength, the first Townsend coefficient depends mainly on the mean free path of the electrons [6]. In this case, the energy gained between two collisions is higher than the ionization energy and the multiplication can be assumed as inversely proportional to the electrons mean free path $(\gamma) \propto \frac{1}{d}$ [6], since each collision leads to multiplication.

For low reduced electric field strength (smaller 20 Volt/torr/cm) the first Townsend coefficient is proportional to the electric field [7].

2.1.1.1 Long term gain stability

The long term gain stability of THGEM or GEM based electron multipliers is mainly related to radiation-induced charging up of the isolator (e.g., FR4) and variation of the gas composition due to outgassing of components, water vapor and residual gases [8]. The variation of the gain due to these effects is related to the gas pressure and the field strength within the holes [9].

Charging up of the isolator substrate causes a decrease in the electric field strength and therefore decreases the gain. The hole geometry and the hole diameter have a great influence on this effect. It typically occurs on a much shorter timescale (under one hour) compared to the change of the gas mixture. To achieve a stable operation of the THGEM, it should

be running for several hours in order for the gas mixture to stabilize (given a constant gas flow) [9]. Impurities in the gas usually decrease the gain (section 2.1.1.3), although very few mixtures may cause an increase of gain (section 2.1.1.2).

2.1.1.2 Penning effect

A mixture of a pure gas with a small amount of quench gas, for which the first excitation level of the pure gas is higher than the ionization energy of the quench gas, is called Penning mixture [10]. For this mixture it is especially easy to create new electron-ion pairs, because the excited state of the pure gas can ionize the quench gas. This can increase the multiplication by several orders of magnitude. Examples for a Penning mixture are neon with argon or helium with nitrogen.

2.1.1.3 Impurities

Residual gases can have different effects, sometimes intended. The Penning effect (2.1.1.2) can be used to increase the total gain of a gas mixture. Other gases (e.g. oxygen) have a high electronic affinity and can capture electrons [11]. This can be a problem, since by capturing electrons spatial resolution and energy resolution is lost - the electron is recombined. This also means the gain is significantly lowered.

During the avalanche process photons are produced (section 2.1.3). In order to capture these photons, complex molecules with many different vibrational and rotational modes can be utilized. The eigenmodes from these molecules (i.e. CO_2 , CH_4) can be excited with a broad range of photons and absorb them [12]. A combination of two gases with these properties, for example helium with carbondioxyde (10%) is common to use for conventional GEM structures in order to capture the photons created during the avalanche process. The

gas regulating the amount of free photons is called a quencher.

2.1.2 Ion feedback

Whenever an electron is generated in an avalanche the corresponding ion drifts in the opposite direction. These ions can, for example, cause a distortion of the electric field, and therefore decrease the spatial resolution. In a photomultiplier, these ions even cause additional waves of electrons whenever they hit a electrode.

It is therefore important to control the ion backflow. This can be done by capturing the ions on the upper layer of the THGEM (section 3.2.4).

2.1.3 Photon feedback

During the avalanche process many photons are produced, mainly due to excitation of the gas atoms instead of ionization. These photons can cause secondary ionization processes in the gas and on the electrodes. In a Penning mixture (section 2.1.1.2) and also in pure gas such a photon can ionize a gas atom.

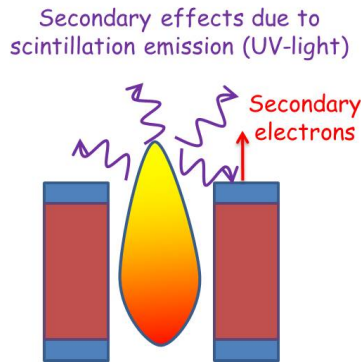


Figure 2.2: Visualization of the secondary emission from the electrode due to photons. Figure taken from [9].

This leads to the creation of many new avalanches. When a photon hits an electrode, an electron can be emitted due to the photoelectric effect (Fig. 2.2). In both cases the spatial

resolution and the energy resolution suffer because the amplification is not proportional to the original signal anymore [13]. A well known method to capture these photons and prevent secondary ionization is to add a quencher (i.e. CO_2 , CH_4) to the gas mixture (section 2.1.1.3). These photons can also be absorbed by the isolator substrate, if the avalanche is confined within the hole.

No matter which way the photons are regulated, the result is a higher maximum achievable gain, because proportional operation is possible at higher voltages. If the photons aren't captured, the avalanche grows exponentially, fed by additional small avalanches, eventually causing a complete ionization of the gas within the hole. The ionized gas then becomes a conductor between the two electrodes, causing a spark and voltage breakdown [13].

2.1.4 Limit of gain

Raether's limit, an empirical value for the maximum avalanche size, is $\alpha d < 20$, meaning a maximum gain of 10^8 [13]. But before this empirical limit is reached, there can be a short circuit due to a conducting band of ionized gas between the two electrodes, when no quench gas is used. This is called streamer mode. Formation of additional avalanches before and after the original one, due to secondary ionization by photons, lead to the streamer mode. The avalanche becomes one long conducting band when the field is deformed due to space charge effects caused by the avalanche itself. The avalanches caused by photon mediated secondary effects then drift towards the existing avalanche, causing it to further grow and deform the field even more. Therefore the formation of streamers is a self enhancing process. It is shown Fig. 2.3. Depending on the gas mixture and geometry this effect can limit the maximum gain significantly by several orders of magnitude [13].

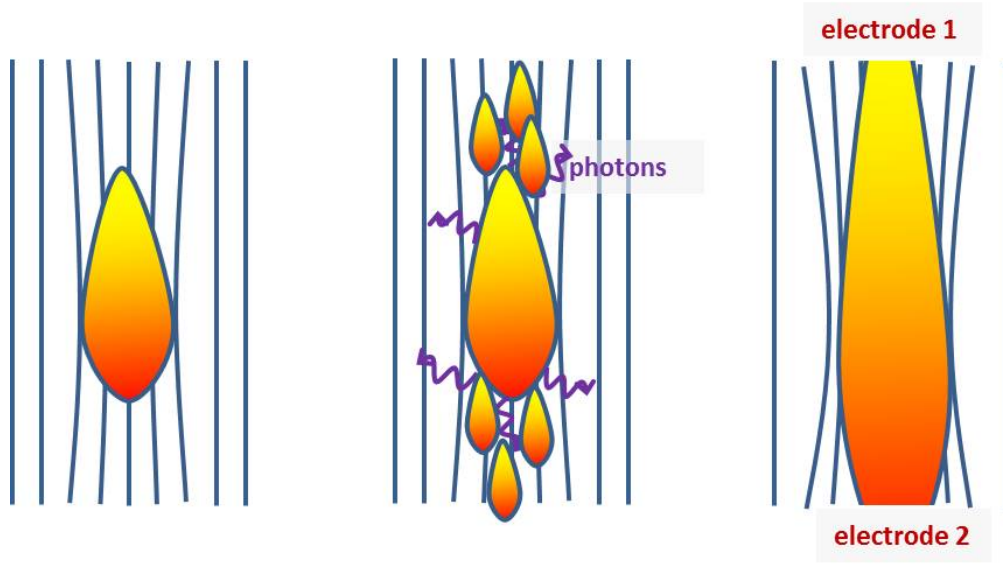


Figure 2.3: Illustration of the formation of streamers and the resulting area of ionized gas (left to right). Inspired by Ref. [13]

2.2 Hole-type detector structures

A schematical drawing of two cascade THGEMs is shown in Fig. 2.4. THGEMs consist of two copper electrodes and a core material (i.e. FR-4, Kapton, Kevlar). Holes are drilled mechanically through these layers, which are produced by multi-layer printed circuit board (PCB) technology. The production process is finished off by chemically etching a small rim (100 μm) around the holes into both outer copper surfaces. Rims have the advantage of reducing the probability of discharge due to mechanical defects and thus increase the gain limit [14]. THGEMs are a lot more robust mechanically and easier to handle compared to micromegas or traditional GEMs, due to their thickness of about 0.6 mm.

Primary electrons are transferred to the THGEM setup by a drift field (E_{drift}). After multiplication in the first THGEM with a voltage difference of ΔV , they are transferred to the second THGEM under the influence of a transfer field (E_{trans}). They are then extracted from the second THGEM by the induction field (E_{ind}). The influence of these fields on the

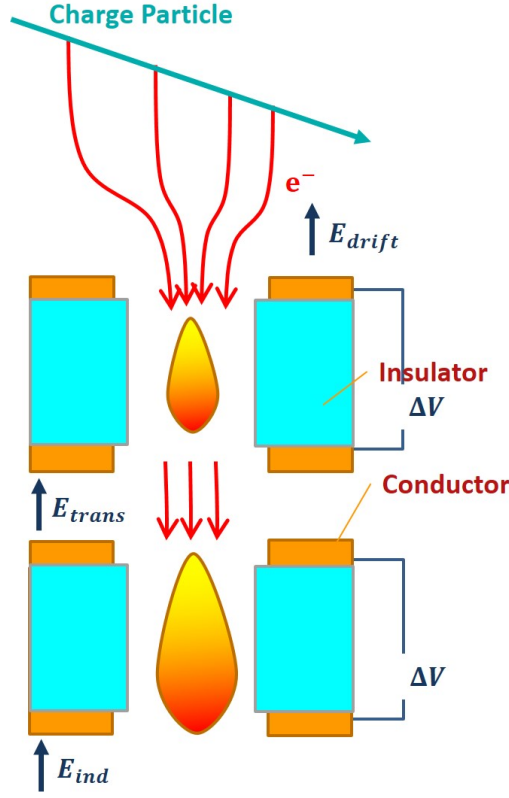


Figure 2.4: Schematic drawing of a two cascade THGEM setup, like it is used in the AT-TPC.

optimum electron gain and minimum ion backflow is important to understand for a successful operation.

2.2.1 Two cascade THGEMs

Two single-layer THGEMs can be combined into a more effective module. By combining them it is possible to achieve the same gain with a smaller voltage across each module compared to that of a single module. The two THGEMs are placed 2 mm apart with a transfer field of $0.25 \frac{\text{kV}}{\text{cm}}$. A portion of the ion backflow from the second THGEM is absorbed by the second THGEM and therefore reduced. In the AT-TPC this setup is combined with a micromegas. The full module is shown in Fig. 2.5. The field strength ratio between the dipole field within the THGEM and the drift field, transfer field and induction field determine the electron collection efficiency, transfer efficiency and extraction efficiency respectively (section

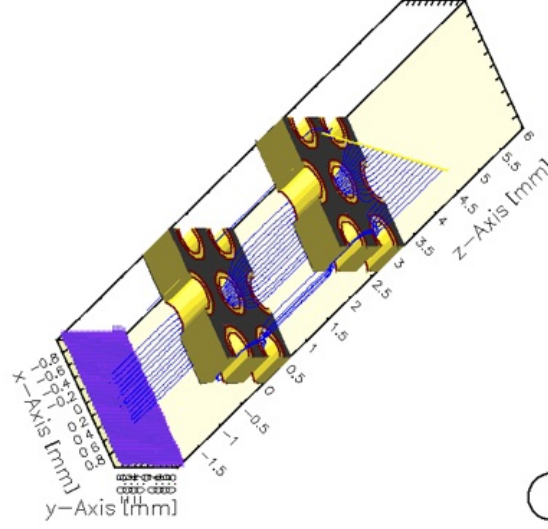


Figure 2.5: Setup of two cascade THGEMs including the micromegas. The image is created in Garfield [5] and shows the drift lines of electrons in vacuum.

3.2.2).

In the AT-TPC the micromegas is located $128\,\mu\text{m}$ above the readout pads. When operating the THGEM as the multiplication device, there is no multiplication necessary within the micromegas. Thus, the transparency of the micromegas can be used to set the gain for every single pad by applying a bias on individual readout pads with the micromegas grounded. Each THGEM consists of a substrate of $0.6\,\text{mm}$ thickness. The copper strata is $0.01\,\text{mm}$ thick. The diameter and pitch of the holes are $0.5\,\text{mm}$ and $1\,\text{mm}$ respectively.

2.2.2 Three-layer M-THGEM

Combining three THGEMs to one single module (three layer M-THGEM) allows for a higher confinement of the avalanche within the hole, which gives a better control over photon-mediated secondary effects. This eliminates the need of a transfer field because all electrons and ions are transferred from one layer to the next. Such a setup is shown in Fig. 2.6. The

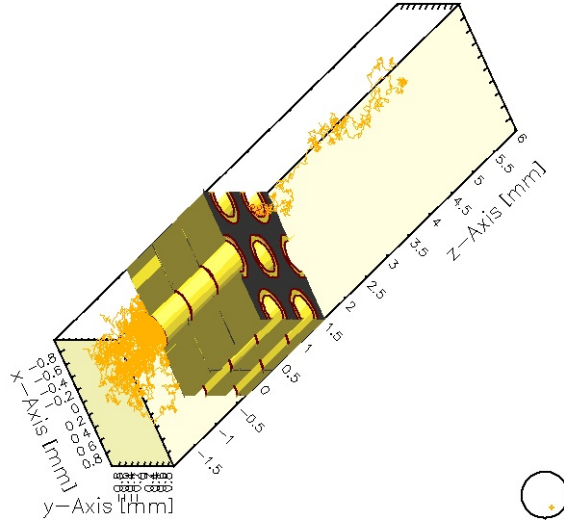


Figure 2.6: Setup of the three layer M-THGEM including the visualization of an avalanche created by a single electron. The image is made using Garfield [5].

module is mechanically sturdy, about 2 mm thick and very robust. The setup can not only be operated with symmetric voltages applied to all layers but also with asymmetric voltages, meaning the first layer acts as an collector and the multiplication happens only in the second and third THGEM (Fig. 2.6).

This presents the advantage that the avalanche can be confined within the M-THGEM (section 2.1.3,5). The dimensions are equivalent to a single-layer THGEM, therefore the total thickness of the three layer M-THGEM is 1.8 mm.

2.3 Signal formation

When charged particles travel through the THGEM, they create a signal in the electrodes they pass by. The induced signal depends on the charge of the particle and its velocity relative to the weighting field.

The Ramo-Shockley theorem describes the current induced in the electrode (I_R) [15]:

$$I_R = -q \cdot E_R^W \cdot \vec{v} \quad (2.1)$$

- I_R current in the electrode
- q electric charge
- E_R^W weighting field of the electrode
- v velocity of the charge with respect to the weighting field

The weighting field is defined as the field induced by one unit of potential (positive) on the readout electrode, when all other electrodes are at zero potential [15].

The induced current integrated over time equals exactly the charge of the particle, in this case an electron.

As a result, the multiplication within the THGEM can be measured, integrating the current induced in one THGEM electrode (the last), given the primary number of electrons is known.

Chapter 3

Simulations

3.1 Field simulation

The electric field has to be calculated before the electron and ion drift can be simulated. Therefore field simulation are performed in ANSYS Maxwell 11 [16]. This electric field data is then used in Garfield [5] to determine the expected multiplication of the THGEMs.

3.1.1 Two cascade THGEMs

Between the two electrodes of one THGEM the field is similar to a dipole field. More precisely two half dipole fields separated by a section with parallel field lines (Fig. 3.1). Far away from the THGEM the drift field has parallel field lines. In Fig. 3.1 the top edge of one THGEM is shown.

An ion drifting away from the avalanche created within the THGEM would follow the field lines shown, depending on its velocity. It is clear that in some cases it will collide with the copper strata where the dipole field lines curve into the surface, in other cases it will leave the THGEM.

Therefore the collection efficiency of ions is determined by the shape of field lines on top of the THGEM, driven by the ratio between the drift field and the dipole field. This ratio also determines the electron collection efficiency. For the transfer field between the

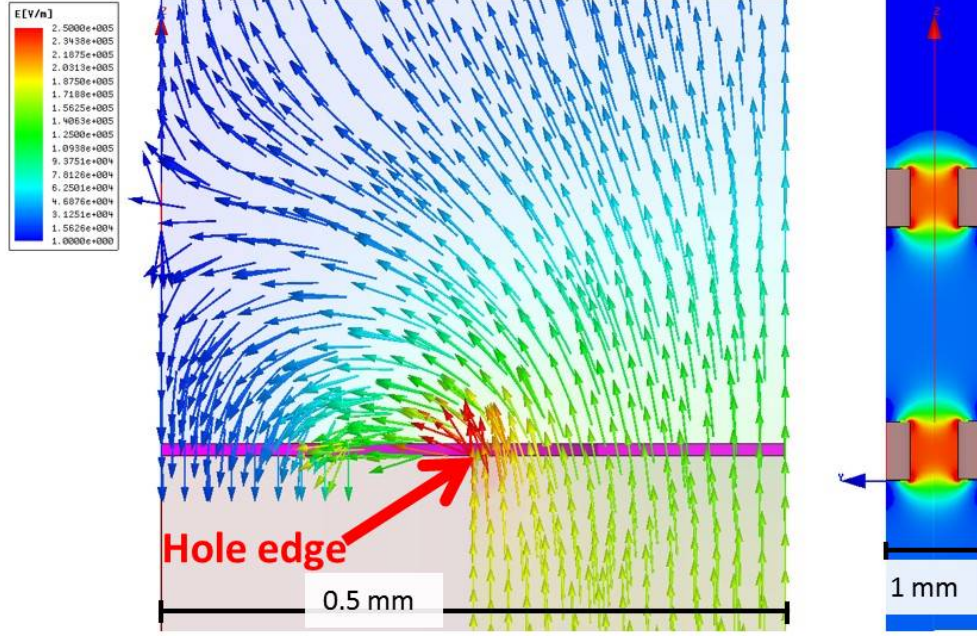


Figure 3.1: Simulation of the electrical dipole field on top of a THGEM (left). Plot of the electrical field magnitudes within the whole structure of two cascade THGEMs. The drift field is set to $0.5 \frac{\text{kV}}{\text{cm}}$, the induction field is set to $1.5 \frac{\text{kV}}{\text{cm}}$ and the transfer field is $1.5 \frac{\text{kV}}{\text{cm}}$. The voltage across one THGEM is 1500 V.

two THGEMs, it is important to find a good compromise between a high electron extraction efficiency using a strong transfer field, combined with a weak dipole field and a high collection efficiency in the second THGEM, which is obtained with a low transfer field and a high dipole field. It would be clear how to determine the optimal transfer field strength in this scenario, but the secondary ionization due to the photon mediated effects also plays a significant role. If the transfer field is too strong, the avalanche extends out of the hole and photons reach the copper substrate, causing the THGEM to transition into non-proportional mode and eventually streamer mode (discharge).

3.1.2 Three-layer M-THGEM

3.1.2.1 Symmetric voltages

For the three layer M-THGEM the difficulties involving the transfer field do not exist, because all electrons and ions are transferred to the next layer. In Fig. 3.2, the simulated

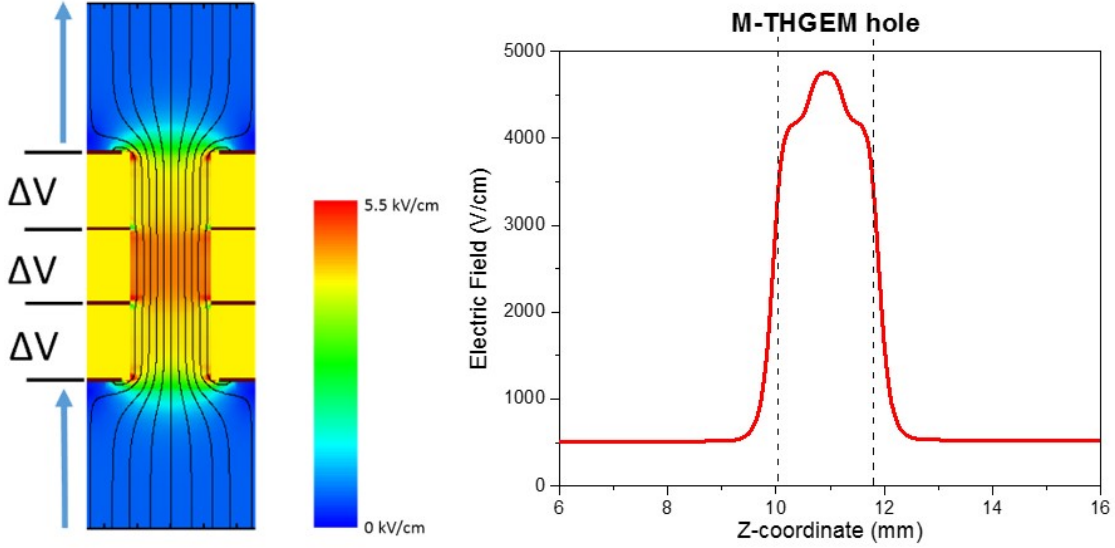


Figure 3.2: Simulation of the electric field strength within a three layer M-THGEM (left). The voltage across all layers of the M-THGEM is the same. Plot of the electric field strength along a vertical cut through the plot on the left, showing the field enhancement in the center of the M-THGEM (right).

field strength within a three layer M-THGEM is shown. It is remarkable that there is a field enhancement within the middle element of the three layer M-THGEM. Since the multiplication scales quadratically within the electric field, this effect confines the avalanche in the middle of the M-THGEM (section 5).

This confinement suppresses the photon mediated secondary effects because all photons are absorbed by the isolator.

3.1.2.2 Asymmetric voltages

In order to achieve an even higher confinement, the three layer M-THGEM can be operated in an asymmetric voltage configuration, where the voltage across the first THGEM is lowered to 3 of the original voltage. This configuration gives the advantage of a completely suppressed photon feedback on the top of the THGEM and a higher ion collection efficiency. It will be discussed in detail in section 5.

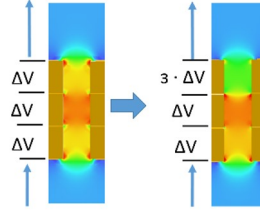


Figure 3.3: Simulation of the field strength within a three layer M-THGEM. On the left, the voltage applied to all layers is equivalent, on the right the top layer is reduced to 3 (70%).

3.2 Particle drift

3.2.1 Range in the AT-TPC

3.2.1.1 SRIM (energy loss calculation)

In order to measure the gain and energy resolution, it is important to know how much energy is deposited in the gas volume by an ionizing particle, such as an alpha particle with 5.5 MeV. Depending on the gas pressure the alpha particle might not be stopped within the gas volume and therefore not deposit its full energy within the active volume. Figure 3.4 shows the energy loss in electron volt per angstrom depending on the distance traveled in the AT-TPC. The rate of the energy deposition increases at lower energy (velocity) of the alpha particle. This Bragg curve will be observed in reverse form, when measuring the energy

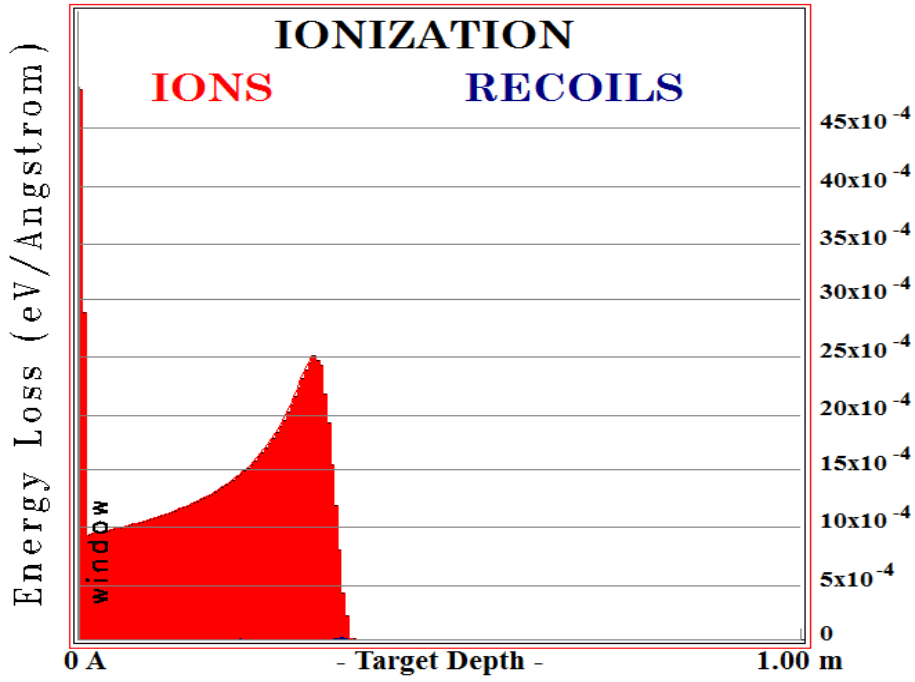


Figure 3.4: Range within the AT-TPC using pure Helium at 400 torr. The energy loss per angstrom is plotted as function of the penetration depth. The $3.6\text{ }\mu\text{m}$ thick para-aramid window is taken into account.

deposition as a function of time. The range simulated in SRIM for different pressures in

pressure	range
200 torr	73.5 cm
400 torr	37 cm
600 torr	24.5 cm

Table 3.1: Range of alpha particles in helium simulated using SRIM

helium is presented in Tab. 3.1. Depending on the angle of emission, an alpha particle will not be stopped within the active volume for a gas pressure of 200 torr and 400 torr, because the radius of the AT-TPC is only 25 cm.

3.2.1.2 MCNPX (alternate energy loss calculation)

For hydrogen, the range of alpha particles is simulated using MCNPX [17]. This software takes the geometry of the detector and the angular distribution of the source into account.

A graphic demonstration of one simulation is shown in Fig. 3.5.

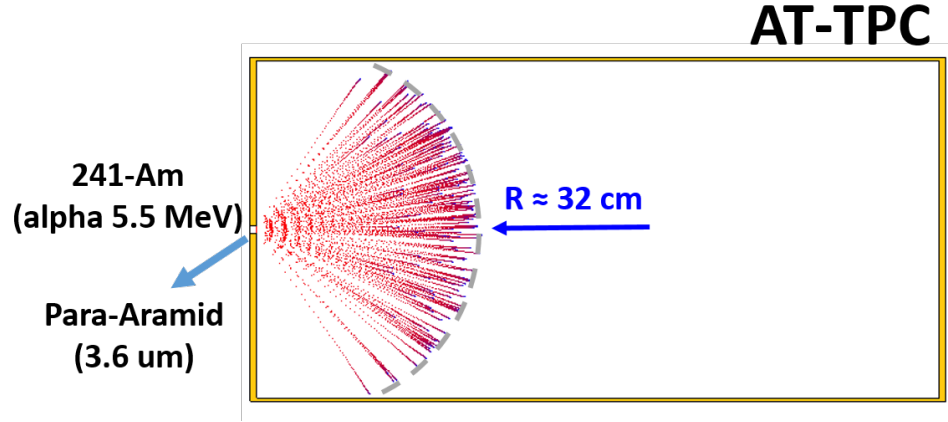


Figure 3.5: Range within the AT-TPC using pure Hydrogen at 400 torr. The resulting energy distribution is shown in Fig. 3.6.

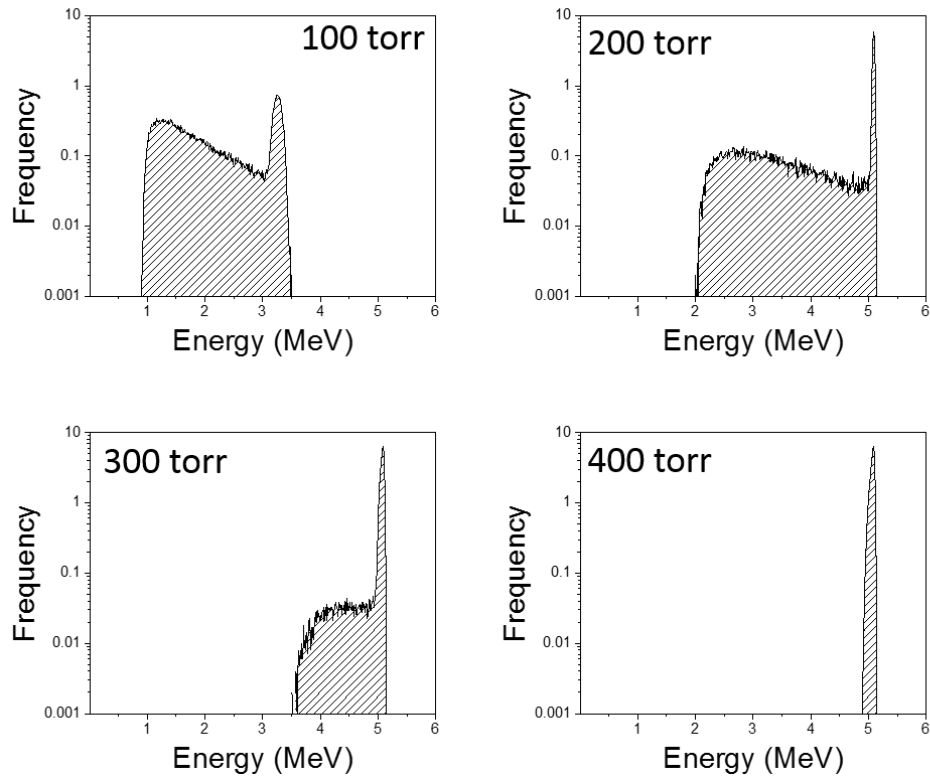


Figure 3.6: Distribution of the energy deposition in hydrogen within the AT-TPC, taking into account the window and angle distribution of the source.

The para-armid window is also included in the simulation. The range in H_2 is a little

bit shorter than in helium. The values for different pressures are shown in Tab. 3.2. Since

pressure	range
200 torr	64 cm
400 torr	32 cm
600 torr	21.5 cm

Table 3.2: Range of alpha particles in hydrogen simulated using MCNPX.

MCNPX also includes the angular distribution in its calculation, it is possible to calculate the expected energy distribution of alpha particles detected in the AT-TPC using an Americium-241 source (Fig. 3.6).

3.2.2 Electron collection efficiency

A high electron collection efficiency is important to obtain full tracks and a good energy resolution. It is mainly determined by the ratio between the drift field and the field at the first layer of the THGEM. Therefore, the collection efficiency is mostly independent of the geometric configuration. Figure 3.7 shows the collection efficiency for different asymmetric voltage configurations of the three layer M-THGEM. In order to obtain each datapoint the drift lines of 200 bunches (each 143 electrons) have been calculated, and the fraction of those entering the THGEM plotted. The error bars are given by the standard deviation of the 200 bunches of electrons. It is clearly visible that with a higher dipole field the collection efficiency increases. For operation in pure hydrogen, the collection efficiency is close to 100% for all drift fields normally used due to the high dipole fields necessary for multiplication. But for helium it can be significant to make sure that the field ratio between the dipole field and the drift field allows for a high collection efficiency, since this will ensure a good spatial resolution, and is essential for the energy resolution. If part of the primary electrons are lost the energy resolution will be degraded.

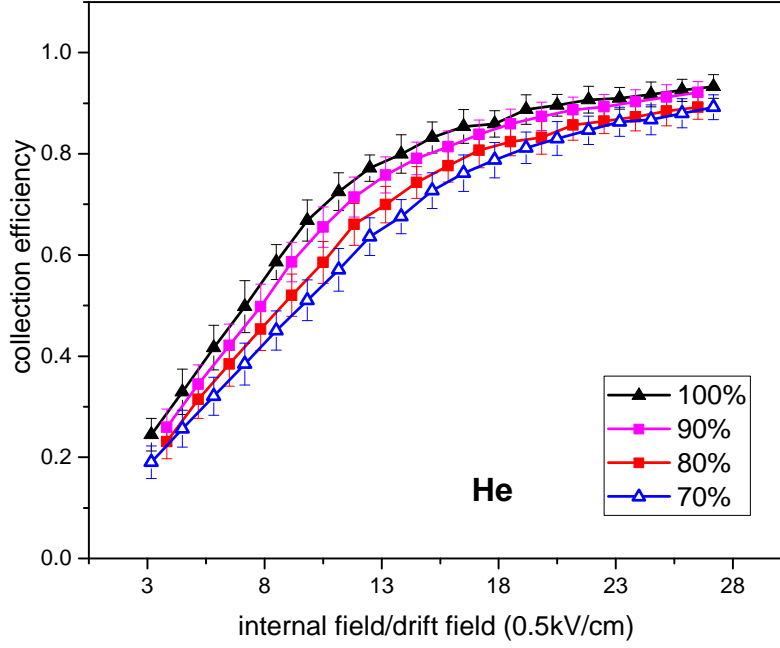


Figure 3.7: Collection efficiency for a three-layer M-THGEM in pure helium at 200 torr. The percentages given describe the potential difference in the first layer compared to the other layers for different asymmetric voltage configuration.

3.2.3 Gain

3.2.3.1 Different geometries and gases

Figure 3.8 gives an overview of all the different geometries and gases used in this work. It shows clearly that a three layer M-THGEM achieves the same gain as a two cascade THGEM with a significantly lower voltage per module. Also, the difference in gain between the symmetric and asymmetric voltage configurations in the three layer M-THGEM is apparent. This overview also shows that for operation in pure hydrogen, the required voltage

is significantly higher. The maximum achievable gain is not given by the end of the curves,

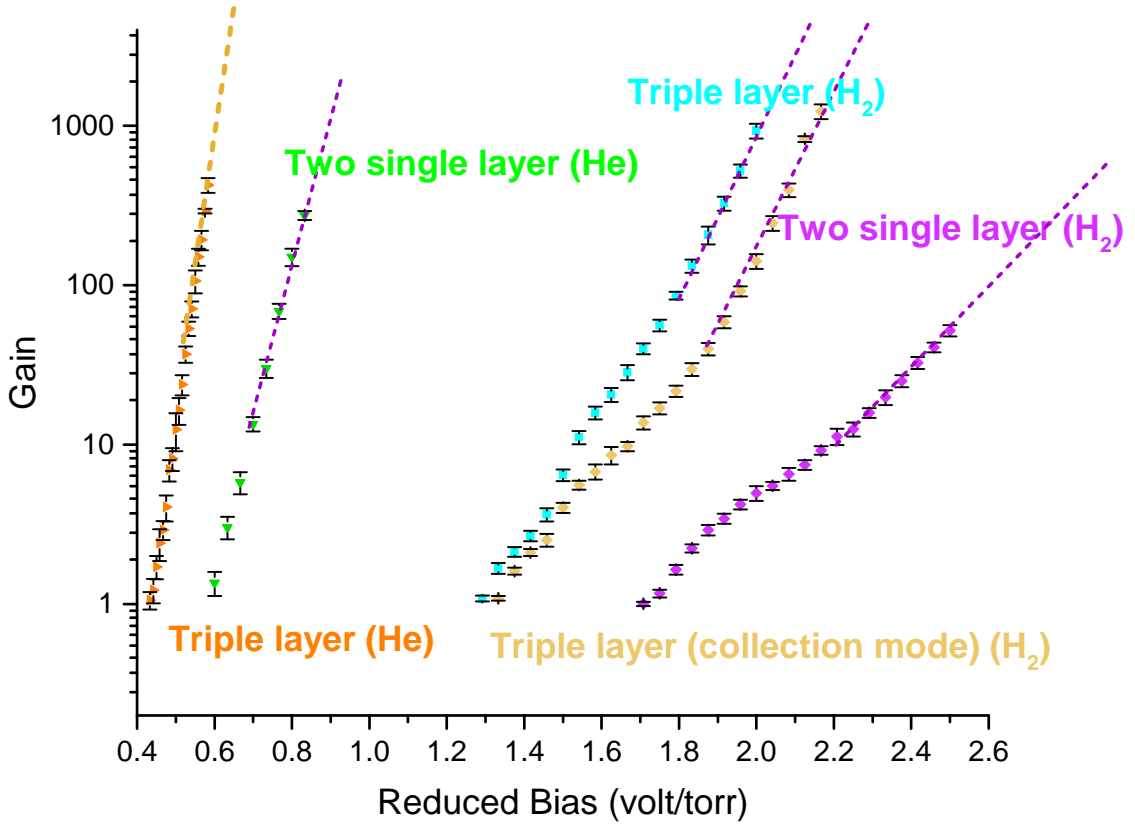


Figure 3.8: Gain curves for all different geometries discussed in this work. The data is generated using garfield [5] at a pressure of 600 torr for all curves.

but rather by the maximum avalanche size, which can be calculated in a reasonable amount of computing time. All gains are plotted against the associated reduced bias, which is the applied voltage to one THGEM element divided by the pressure in torr.

3.2.3.2 Two cascade THGEMs

For each datapoint a total of 1000 complete avalanches were simulated, tracking every ion and electron produced in the avalanche. The routine “avalanche” was used in Garfield [5]. The 1000 avalanches were split into 10 bunches of 100 avalanches. The error shown is given

by the standard deviation of these 10 bunches. The electric field map was first calculated in

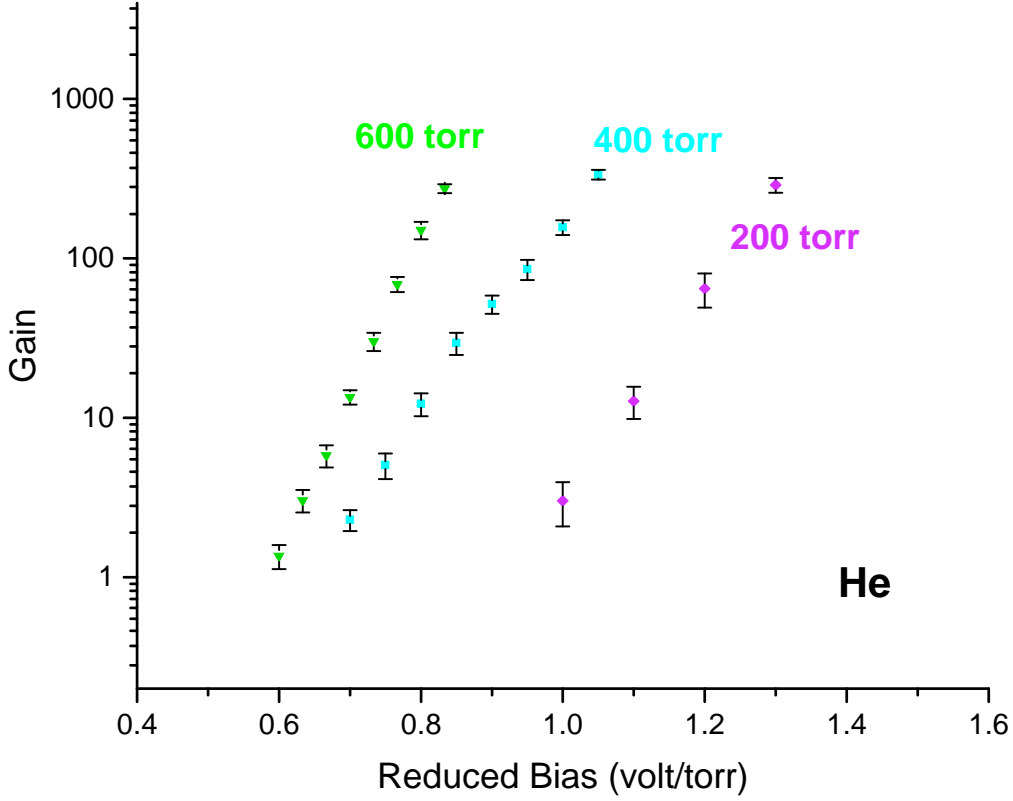


Figure 3.9: Gain curves for different pressures in pure helium, using a transfer field of $0.25 \frac{\text{kV}}{\text{cm}}$ and an induction field and drift field of $0.5 \frac{\text{kV}}{\text{cm}}$.

Maxwell, then the gas drift data modeled in Magboltz, and finally the actual drift performed in Garfield [5]. It is important to use the right unit cells, with the correct symmetries and a suitable integration step. It is also important to use a narrow enough mesh for the finite element simulation in Maxwell. A complete manual on how to perform the simulations is given in the appendix (section C).

Garfield does not include the effect of photon mediated feedback, a quencher or the Penning effect. Therefore these simulations do not fully model reality. When comparing

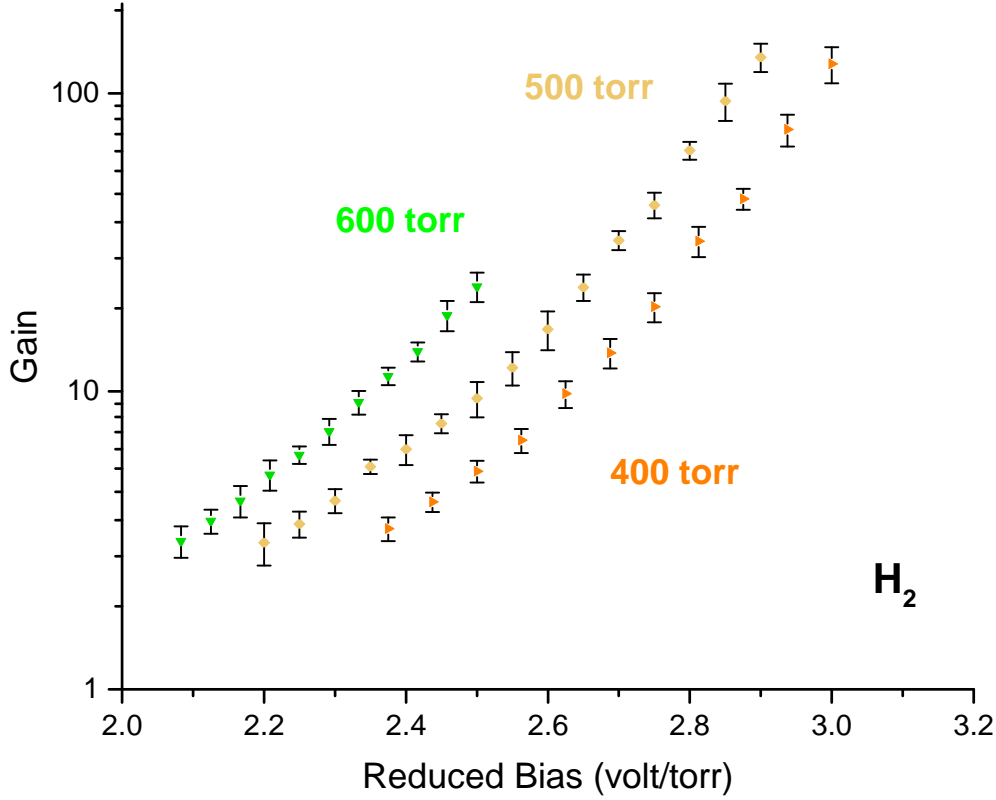


Figure 3.10: Gain curves for different pressures in pure hydrogen, using a transfer field of $0.25 \frac{\text{kV}}{\text{cm}}$ and an induction field and drift field of $0.5 \frac{\text{kV}}{\text{cm}}$.

the simulated results for pure helium to the measurements (section 4), the simulation using helium (Fig. 3.9) shows a significantly lower gain, most likely due to a residue of nitrogen in the active volume. Nitrogen and helium are a Penning mixture (section 2.1.1.2), thus already small amounts of nitrogen can significantly increase the gain.

When comparing the results for hydrogen to the measurements (section 4), the opposite is observed. The simulated gains (Fig. 3.10) are a lot higher than the measured ones, most likely due to residual oxygen in the active volume from outgassing of components or leaks, because oxygen functions as an electron capturing gas (section 2.1.1.3). A direct comparison

for both gases is given in the appendix (section A).

These deviations aside, the simulations show the expected exponential behavior very well, and from the small spread of the gain for a single value (error bars), it can be assumed that the energy resolution is potentially very good.

The values for the fields were set to values common for the AT-TPC to give an impression of the gain to be expected in operation (transfer field = $0.25 \frac{\text{kV}}{\text{cm}}$, induction field and drift field = $0.5 \frac{\text{kV}}{\text{cm}}$).

3.2.3.3 Three-layer M-THGEM

The simulations for the three layer M-THGEM are done in exactly the same way as for the two cascade THGEMs, except from using a different geometry. In this case, the values for the drift field and induction field were set to ensure optimal operation. When examining the presented results, it is important to keep in mind that they do not show any information about the maximum achievable gain. The three layer M-THGEM has a lower gain than the two cascade THGEMs for the same total voltage difference, because the first THGEM layer operates mainly as an electron collector.

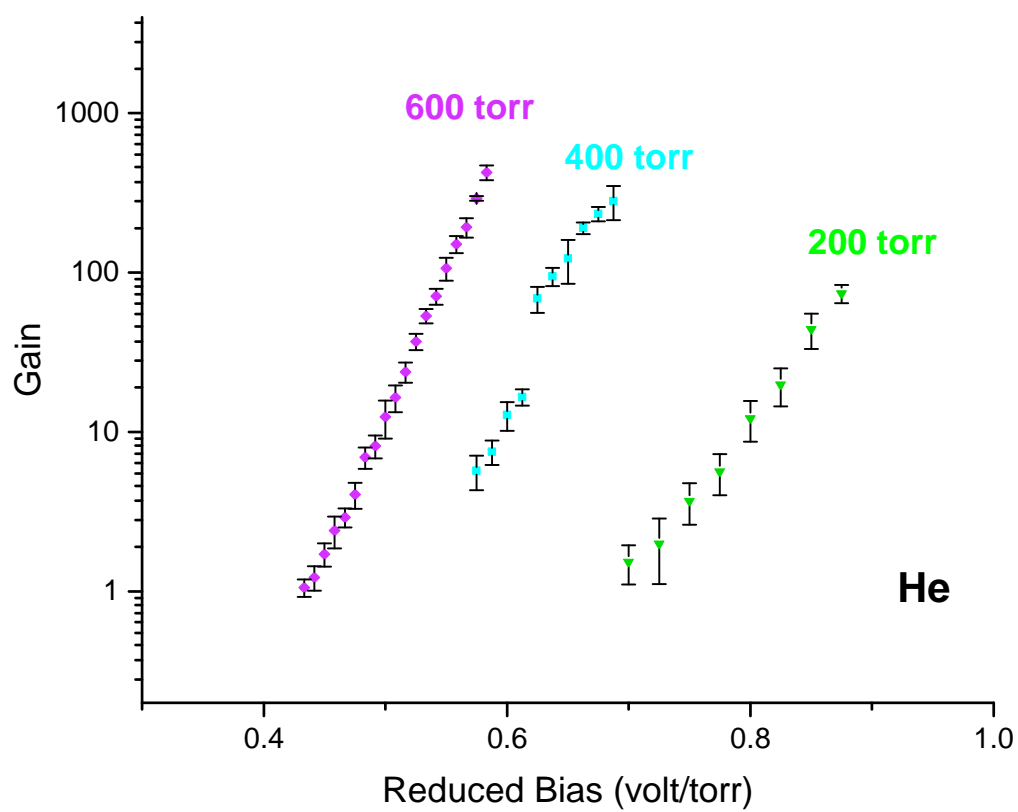


Figure 3.11: Gain curves for different pressures in pure helium, using an induction field and drift field of $0.5 \frac{\text{kV}}{\text{cm}}$.

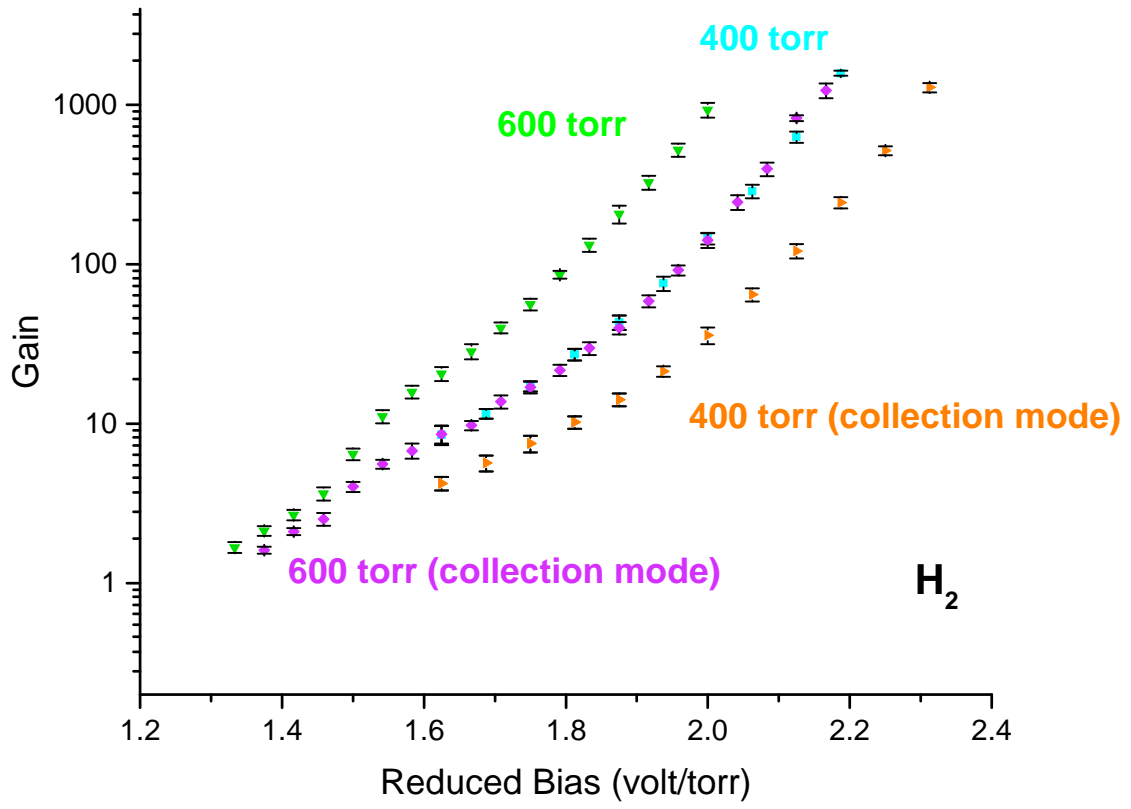


Figure 3.12: Gain curves for different pressures in pure hydrogen, using an induction field of $1.5 \frac{\text{kV}}{\text{cm}}$ and drift field of $0.1 \frac{\text{kV}}{\text{cm}}$. The graph includes gains for the two different operation modes, symmetric voltages and asymmetric voltages (first THGEM 70%).

3.2.4 Ion backflow

3.2.4.1 Transfer field and ion feedback

For the following discussion, the ion backflow (IBF) is defined as the number of ions collected at the cathode divided by the number of electrons at the anode.

$$\text{IBF} = \frac{\# \text{ ions at cathode}}{\# \text{ electrons at anode}}$$

The detector pads are the anode. The simulations for the ion backflow are performed similar to the ones for the gain, but here it is important to give Garfield [5] the correct experimental values for the transport properties of gaseous ions since these are not provided by Magboltz. The ion drift data was obtained from Ref. [18] and Ref. [19]. Figure 3.13 shows the

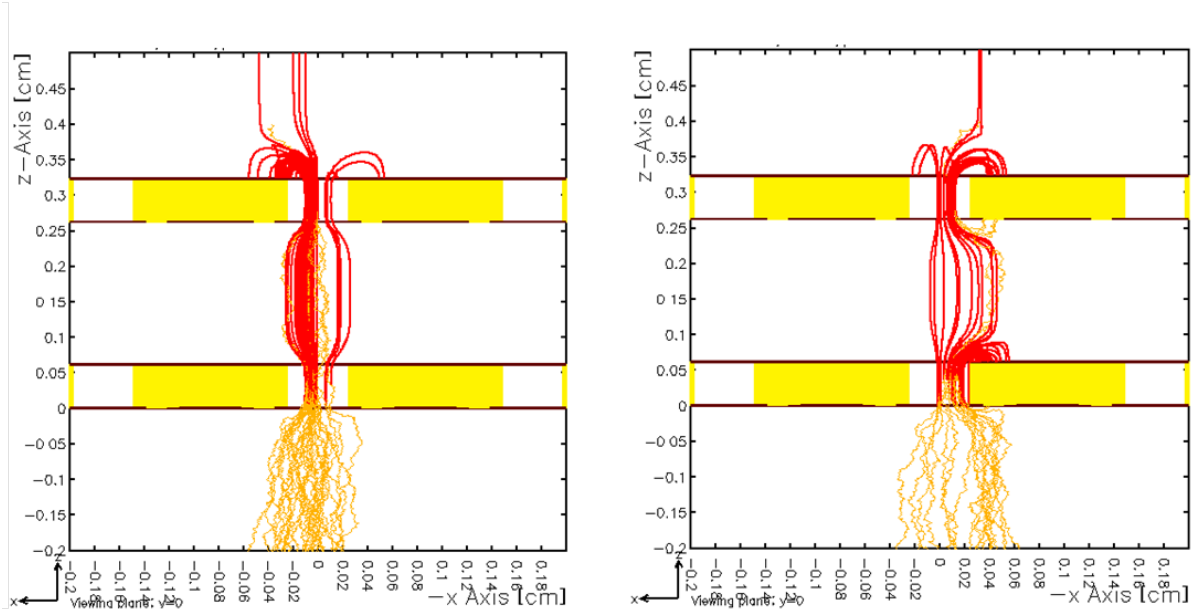


Figure 3.13: Plot of the ion tracks (red) and electron tracks (orange) in one avalanche for a setup with two cascade THGEMs. The plots are generated in H_2 at 400 torr with a voltage of 1025 V across each THGEM using garfield [5]. The potential differences are: drift field $0.1 \frac{\text{kV}}{\text{cm}}$, induction field $1.5 \frac{\text{kV}}{\text{cm}}$, transferfield $1.5 \frac{\text{kV}}{\text{cm}}$ (left) and $0.125 \frac{\text{kV}}{\text{cm}}$ (right).

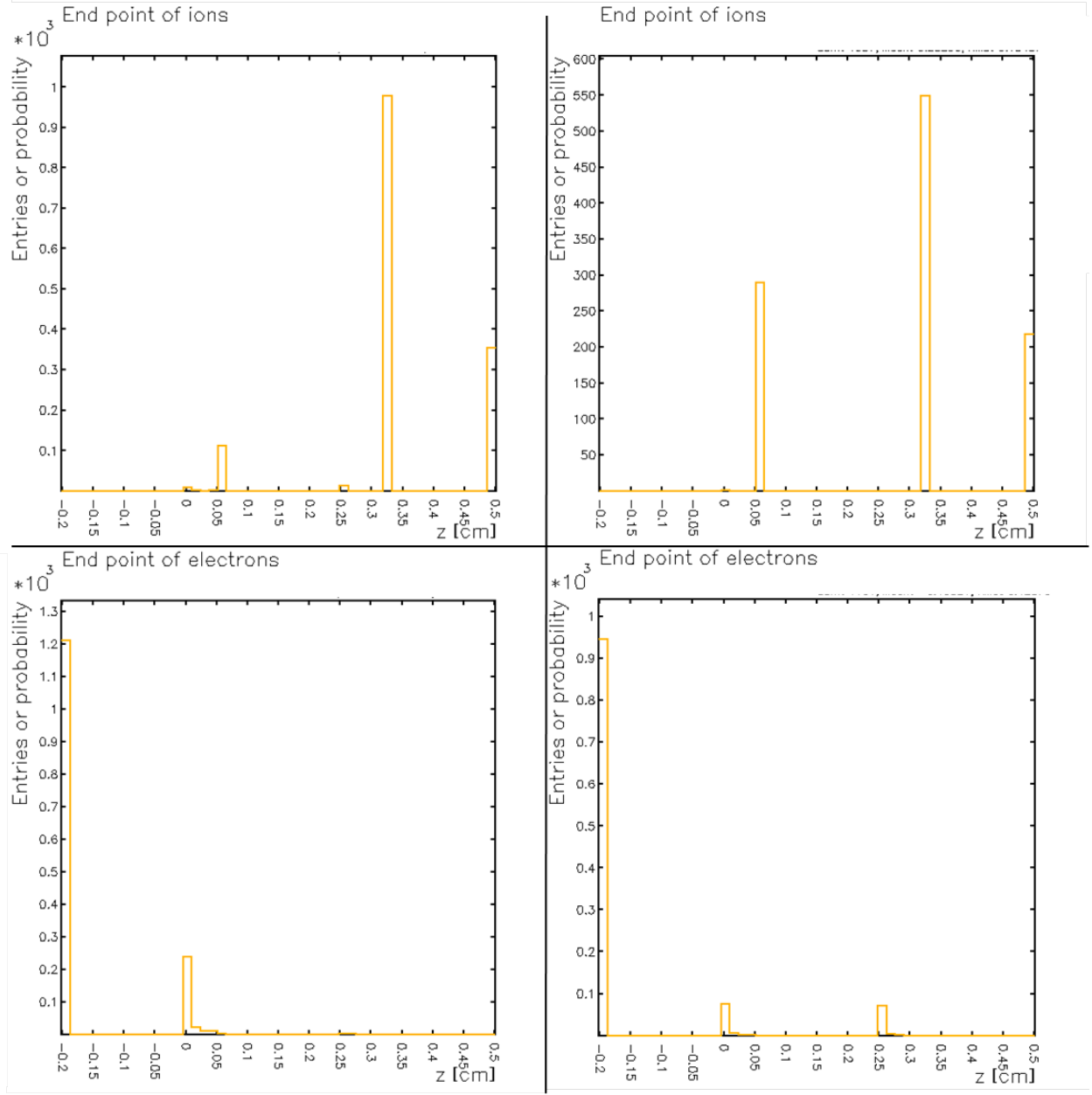


Figure 3.14: Corresponding to Fig. 3.13 the histograms on the left show the endpoints for ions and electrons using a high transfer field, whereas on the right these values are shown for a weak transfer field.

2D plot of one single avalanche (electrons in orange, ions in red). The isolating substrate (yellow) is between the copper strata (brown). Not every layer shows the hole because of the 2D projection, thus showing the whole outer rim of the hole. The figure clearly shows the influence of the transfer field, like mentioned in section 3.1.1. A very high transfer field

($1.5 \frac{\text{kV}}{\text{cm}}$) transfers all ions and electrons. In that case the ions are collected only on top of the first THGEM. In between the two THGEMs the transfer field is relatively strong compared to the dipole field. For a low transfer field ($0.125 \frac{\text{kV}}{\text{cm}}$) ions are also collected on top of the second THGEM, but since the extraction efficiency for electrons from the first THGEM is then lower as well, some electrons are lost. So overall the ion backflow is not reduced, just the overall gain is lowered.

The statistics on where electron and ion paths end is shown in Fig. 3.14. The statistics is done only for 10 avalanches, and the total number of electrons shown is a absolute value (to evaluate the quality of the statistic).

To put this simulation into perspective, one should verify that the applied strong transfer field does not cause the avalanche to extend from the hole. This would lead to photon mediated secondary ionization and transition into the non-proportional mode.

3.2.4.2 Influence of the relative alignment between the two THGEMs on electron and ion transfer

In the setup using two cascade THGEMs, the holes are not necessarily aligned. In the present setup of the AT-TPC they are not aligned. When this is the case the transparency for charged particles is lowered, strongly depending on the distance between the two THGEMs and the gas pressure. In simulations performed by Bin-Long et al. [20] it has been shown that the alignment of the THGEMs makes a significant difference in the ion backflow.

However, this is not the case for the present setup. All ions/electrons are transferred independent of the alignment due to the large hole diameter and long distance between the two THGEMs in comparison to the electrons mean free path (γ). This can be visually seen in Fig. 3.15 and Fig. 3.16 where not a single electron is lost on top of the second THGEM,

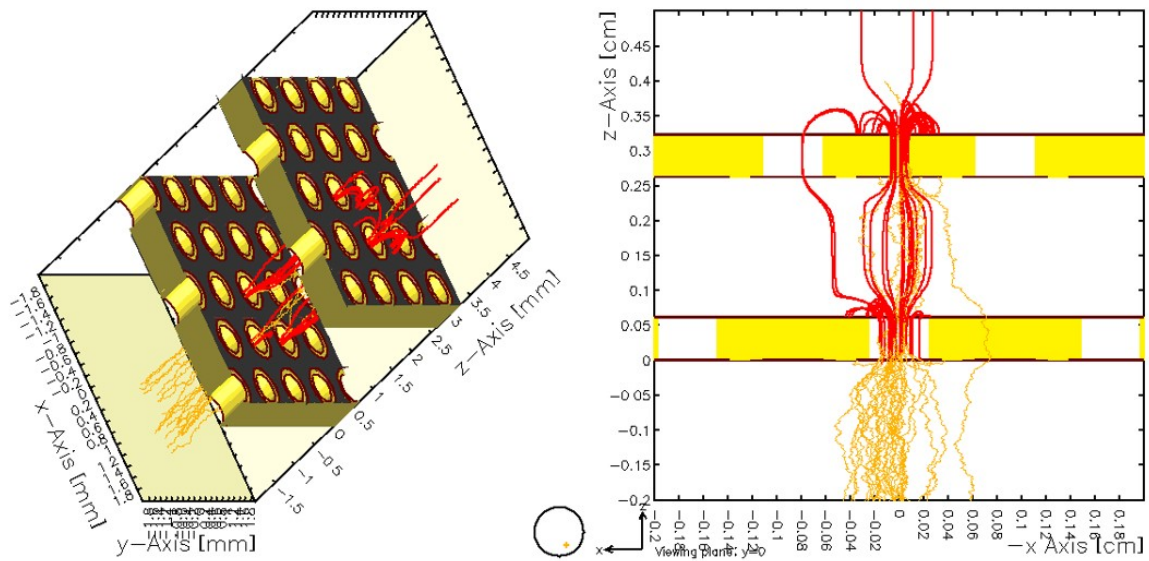


Figure 3.15: Plot of the ion tracks (red) and electron tracks (orange) in one avalanche for two cascade THGEMs, which are not aligned. The plots are generated in H_2 at 400 torr with a voltage of 1050 V across each THGEM using garfield [5]. The drift field is set to $0.1 \frac{kV}{cm}$, the transferfield is set to $0.125 \frac{kV}{cm}$ and the induction field is $1.5 \frac{kV}{cm}$. The left picture shows a 3D view and the right diagram a 2D illustration.

where it could possibly “crash” into the second THGEM due to the misalignment. In the 2D graph of Fig. 3.15, it is important to keep in mind that the ions and electrons which seem to go through the material are actually going through a hole behind the front.

3.2.4.3 Collection of Ions in the three-layer M-THGEM

Since there is no transfer field in the three layer M-THGEM, rather the THGEMs are directly attached to each other, all ions and electrons are transferred independent of the applied voltages, as long as they are applied symmetrically. One single event (avalanche) is shown in Fig. 3.17 to illustrate this behavior.

Looking at the statistics for 1000 electrons, comparing the three layer M-THGEM in collector mode (asymmetric voltages) and symmetric voltages, it is remarkable that a small

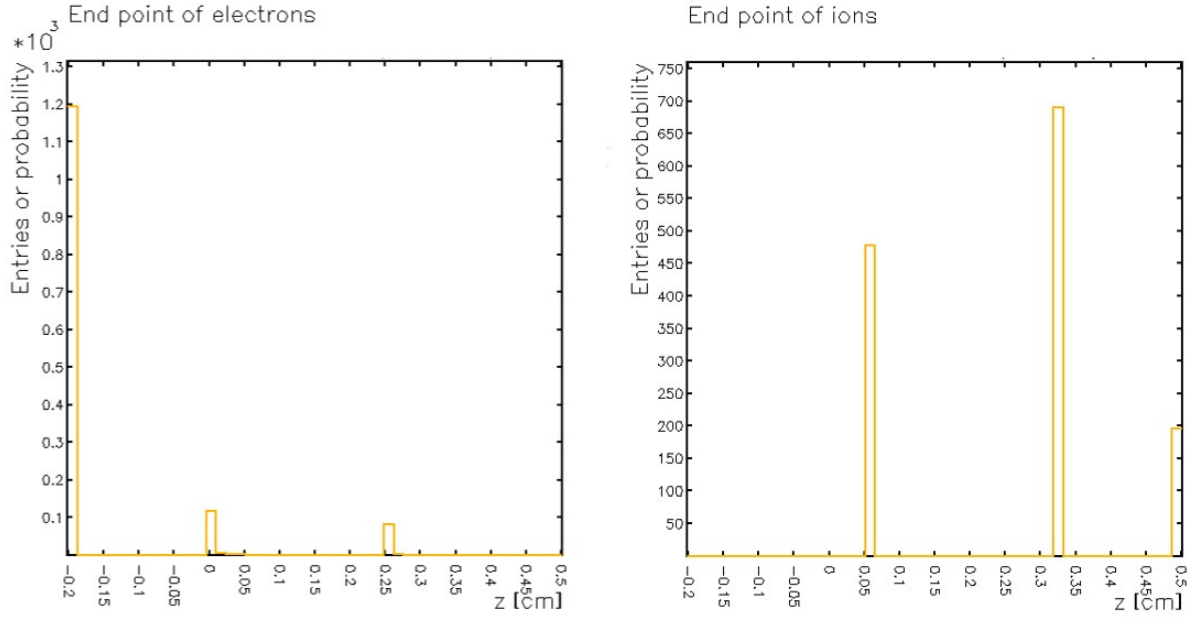


Figure 3.16: Statistics of the endpoints for ions (right) and electrons (left) in the two cascade THGEMs, which are not aligned like shown in Fig. 3.15. The plots are generated in H₂ at 400 torr with a voltage of 1050 V across each THGEM using garfield [5]. The drift field is set to $0.1 \frac{\text{kV}}{\text{cm}}$, the transferfield is set to $0.125 \frac{\text{kV}}{\text{cm}}$ and the induction field is $1.5 \frac{\text{kV}}{\text{cm}}$.

fraction of ions is actually absorbed within the three layer M-THGEM in collector mode, whereas all electrons are still transferred.

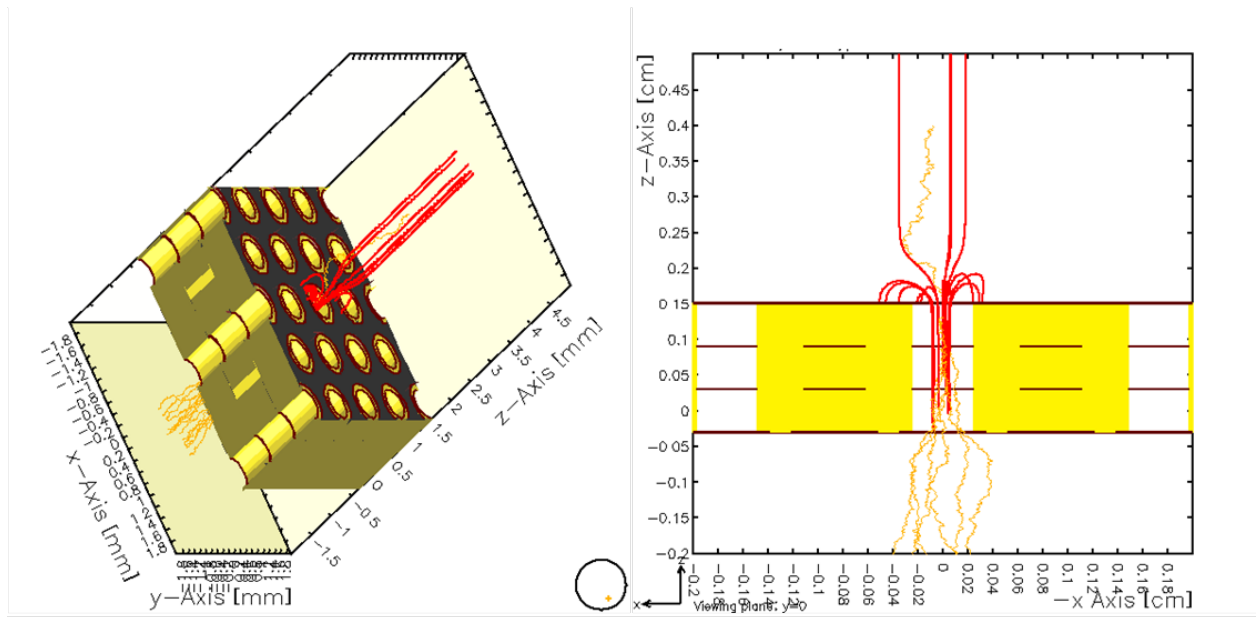


Figure 3.17: Plot of the ion tracks (red) and electron tracks (orange) in one avalanche for a three-layer M-THGEM. The plots are generated in H_2 at 400 torr with a voltage of 650 V across each THGEM using garfield [5]. The drift field is set to $0.1 \frac{\text{kV}}{\text{cm}}$ and the induction field is $1.5 \frac{\text{kV}}{\text{cm}}$. The left picture shows a 3D view and the right diagram a 2D illustration.

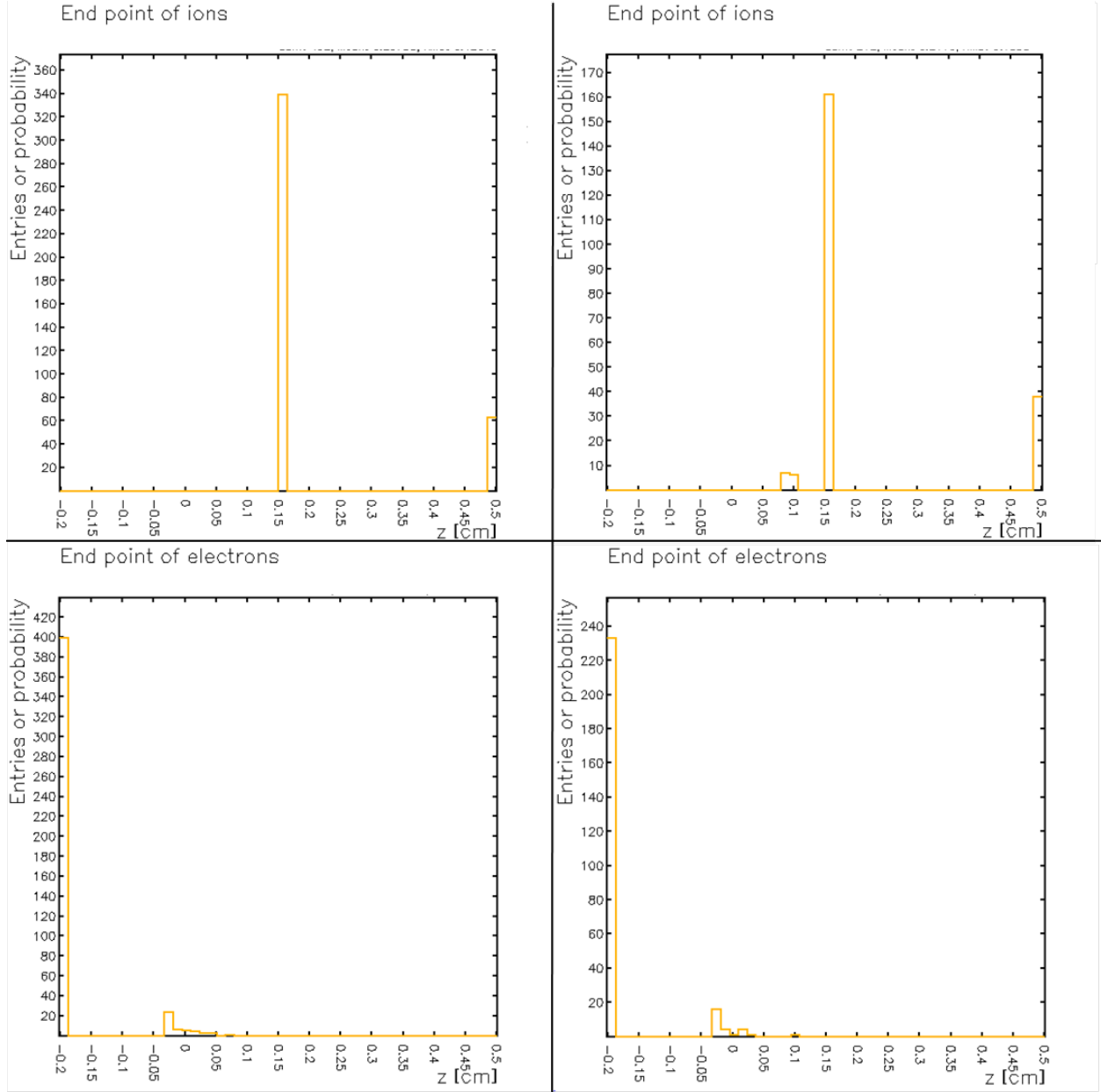


Figure 3.18: Corresponding to Fig. 3.17 the histograms on the left show the endpoints for ions and electrons using a high symmetric voltage of 650 V for each THGEM, whereas on the right the first THGEM is working as a collector (asymmetric voltage configuration). It is set to 70% of the full voltage.

3.2.4.4 Ionfeedback vs. Gain for different configurations

Figure 3.19 displays the ion backflow versus the gain. It shows that the three layer M-THGEM is better than the two cascade THGEMs in terms of low ion backflow. The three layer M-THGEM in collector mode provides the lowest ion backflow. The advantages of this new generation of detectors are discussed in section 5. For the two cascade THGEMs it

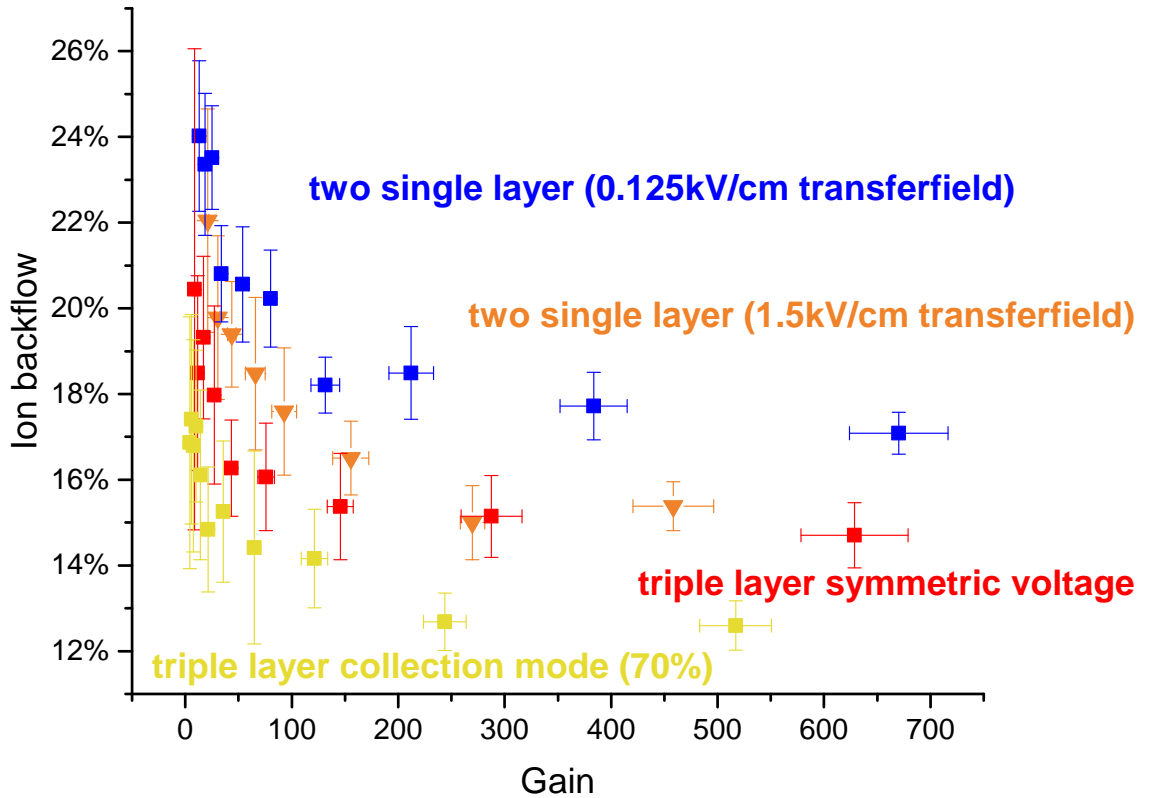


Figure 3.19: Ion backflow (number of ions at the cathode over number electrons at the anode) plotted against the gain for a three-layer M-THGEM and two cascade single layer THGEMs in H_2 at 400 torr. The decrease in IBF for higher gain is clearly visible for each setup. The error is indicated as the $\sigma/2$ spread of the simulation.

is interesting that the high transfer field (collection on top of the first THGEM only) has actually a lower ion backflow than the configuration with the low transfer field (collection

on both THGEMs). This is due to the fact that in case of the low transfer field, electrons are also lost (which would otherwise be multiplied in the second THGEM), and therefore the gain is lower.

Chapter 4

Measurements for the two cascade THGEMs

4.1 Experimental Setup

The experimental setup consists of the AT-TPC detector (Fig. 1.1), which has a radius of 25 cm and a length of 100 cm. There is a thin para-aramid film ($3.6\,\mu\text{m}$) window within the cathode to which a collimated Americium-241 alpha source is attached. Two cascade THGEMs are mounted at the anode, while the second layer of the second THGEM is connected to the readout electronics. The gas pressure can be regulated within the active volume. The drift field can be set using a high voltage power supply.

4.1.1 Gas handling system

The gas handling system is custom made and consists of a Datametrics Dresser 1404 valve controller and an electronic multimeter (1400 Datametrics) to regulate the pressure within the detector vessel and a second equivalent setup to control the nitrogen pressure in the outer volume. The constant gas flow is regulated by a flowmeter connected to the vacuum line for both volumes.

4.1.2 Voltage power supplies

The high voltage source for the experiment is a Heinzinger PNChp 100000-1 neg power supply, connected to the cathode.

4.1.3 Readout electronics

To measure the gain, the signal induced in the last THGEM is used (section 2.3). This signal is integrated using a charge amplifier ORTEC Model 109A. This charge measures the number of collected electrons. Figure 4.1 shows the calibration curve for the charge amplifier, measured using a RC-circuit with a 3.3 pF capacitor and a function generator. The integrated signal is digitized using a FASTER module [21]. The FASTER analog-to-digital converter (ADC) provides different options, including puls-shaping ($33\mu\text{s}$ constant), fast data recording and buffering to record a large number of single events. It is possible to add a linear integration or use it as a multi-channel analyser.

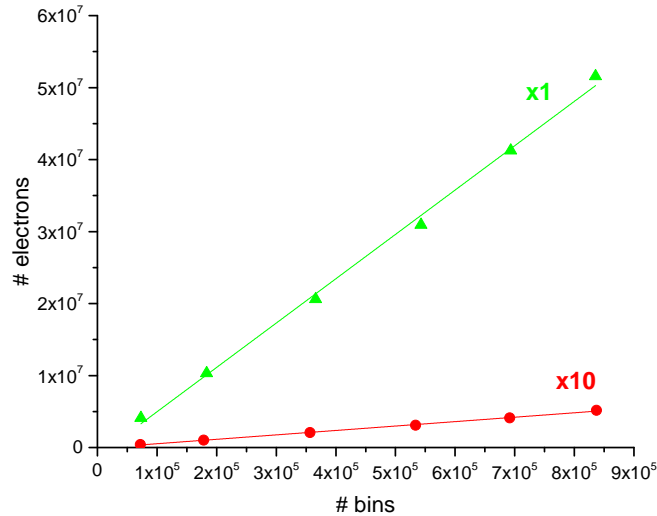


Figure 4.1: Calibration curves for the charge amplifier for the two different amplifications. The slope of the two curves are $6 \frac{\text{electrons}}{\text{bin}}$ and $60 \frac{\text{electrons}}{\text{bin}}$ respectively.

4.2 Performance in Helium

4.2.1 Gain

Using the FASTER module as multi-channel analyzer the peak of the signal is measured and converted to a number of electrons using the calibration. Analyzing the simulation given

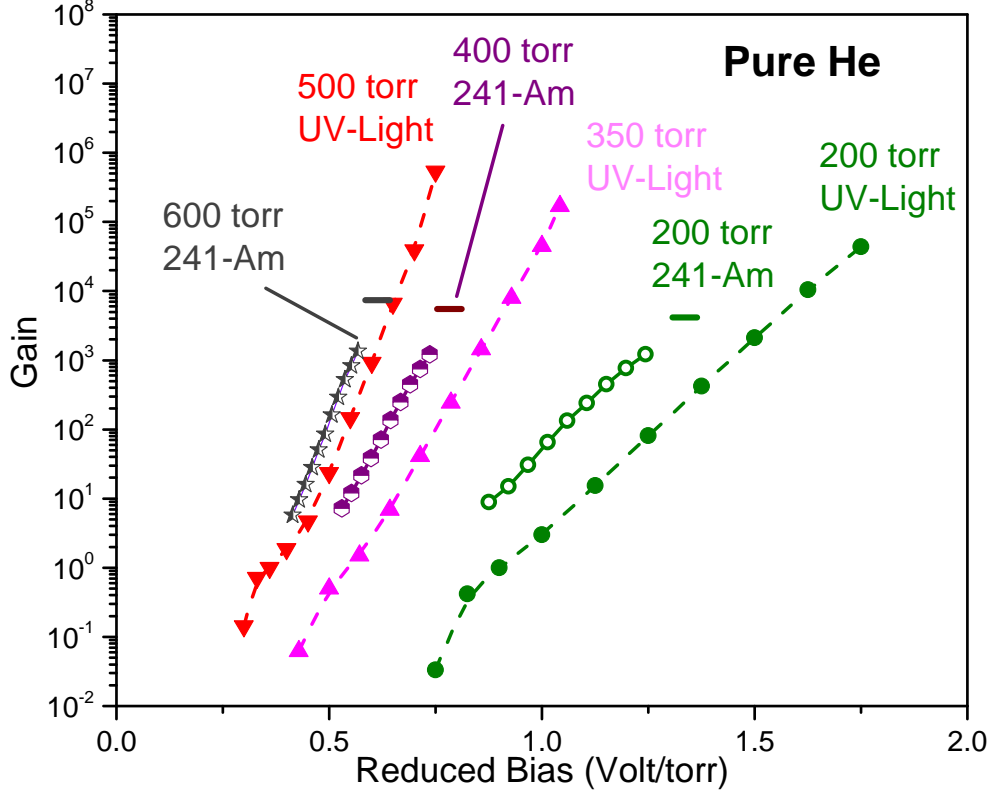


Figure 4.2: Comparison of the gain in pure helium for different pressures. The horizontal lines indicate the maximum achievable gain. In addition three measurements by Marco Cortesi [9] using UV-Light are included.

by SRIM (section 3.2.1.1), the average energy loss in the window is $48 \cdot 10^{-4} \frac{\text{eV}}{10^{-10} \text{ m}}$ with a thickness of $3.6 \mu\text{m}$ (the thickness is smaller than the histogram interval of SRIM (1 cm)) therefore the total energy loss within the window is 0.48 MeV. The total energy loss in the gas is therefore 5.02 MeV (alpha particle fully stopped). Using the ion-electron pair production energy of 46.3 eV given in Ref. [22], the number of primary electrons is about 108,000. The

effective gain was calculated using this number. The main errors are due to the calibration of the readout electronics and the angular distribution of the source. Also, there might be some residual gas, which can modify the gain.

4.2.2 Energy resolution

Two thousand events were recorded using the FASTER module. They are shown in Fig. 4.3. One alpha particle events and two alpha particle events, meaning two arriving at the

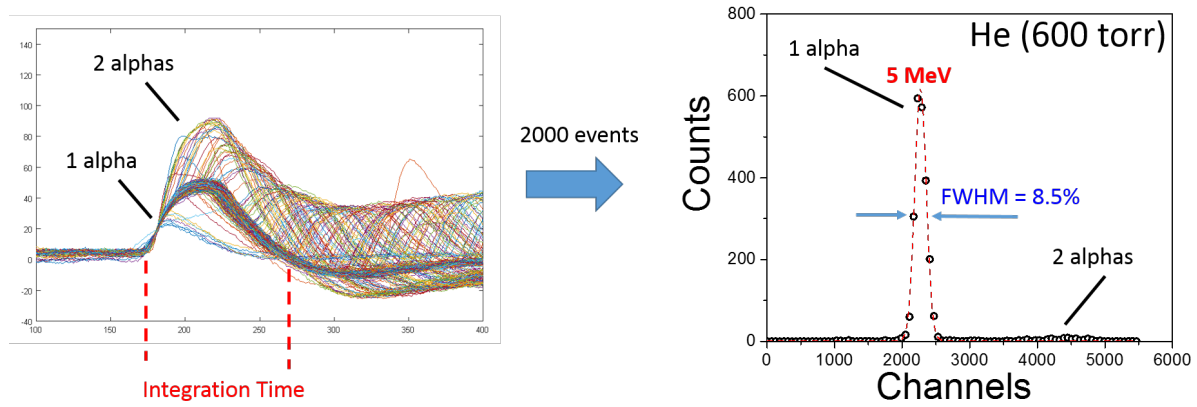


Figure 4.3: Visualization for 2000 events in helium at 600 torr (left). The energy spectrum calculated from these events (right).

same time (overlapping), are clearly visible. The FWHM of the distribution is 8.5%, when constructing the histogram from integrated signal for each single event. That doesn't mean the energy resolution is 8.5% because the energy distribution itself has also a width, but the energy resolution is at least 8.5%. The integration time is marked in red. The main error in this case is the trigger as well as the above mentioned.

4.3 Performance in Hydrogen

4.3.1 Gain

Similarly to the procedure with helium, the same calculation can be done for hydrogen using the energy deposition calculated by MCPNX and shown in Fig. 3.6.

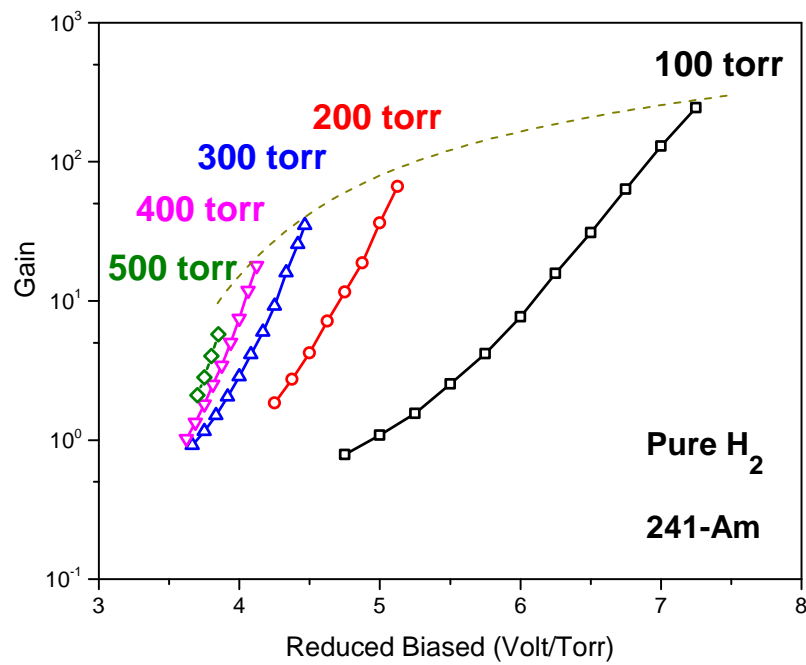


Figure 4.4: Comparison of the gain in pure hydrogen for different pressures. The endpoint of each curve indicates the maximum achievable gain at that pressure.

4.3.2 Electron drift velocity

Using the time measurements in Fig. 4.5. The drift velocity can be calculated. It is difficult to determine the exact pulse length for this data, so the error is at least $\pm 10\%$.

pressure	drift velocity
100 torr	$10 \cdot 10^{-5} \frac{\text{cm}}{\text{sec}}$
200 torr	$9.14 \cdot 10^{-5} \frac{\text{cm}}{\text{sec}}$
300 torr	$9 \cdot 10^{-5} \frac{\text{cm}}{\text{sec}}$
400 torr	$8 \cdot 10^{-5} \frac{\text{cm}}{\text{sec}}$

Table 4.1: Drift velocity of electrons in hydrogen according to Fig. 4.5.

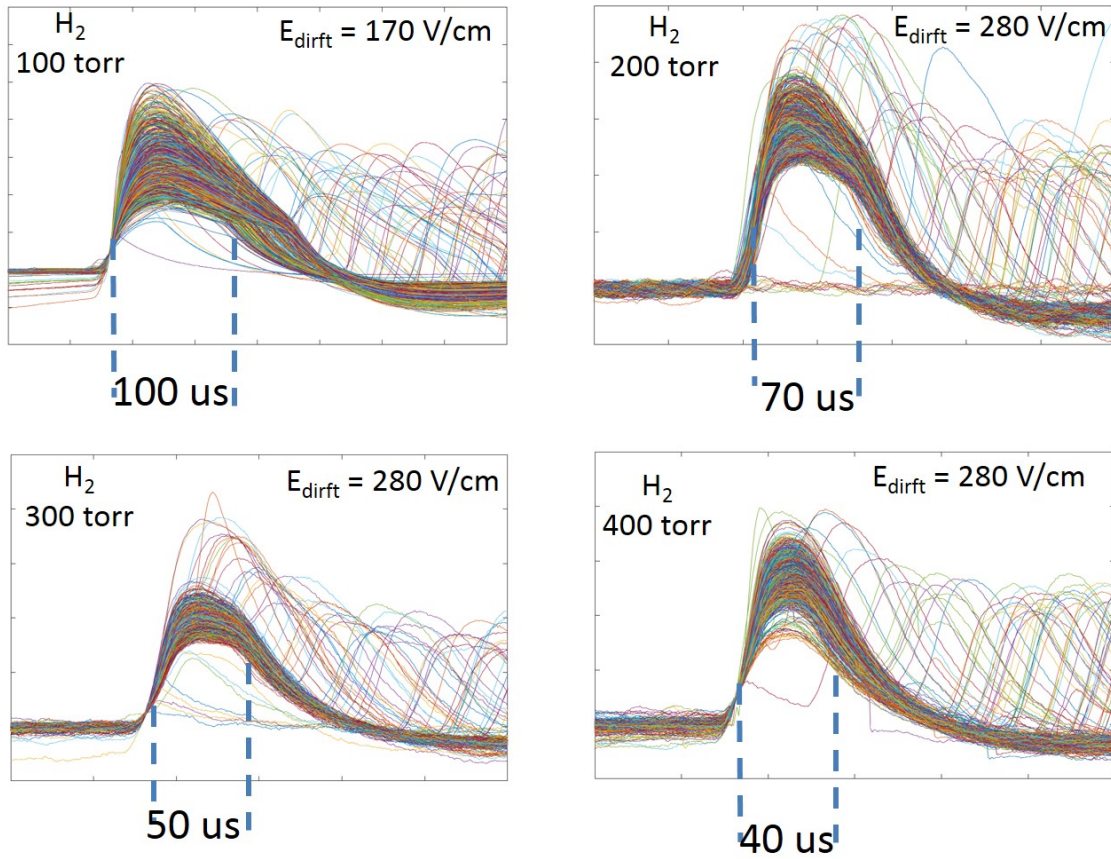


Figure 4.5: Visualization of 1000 events in hydrogen for different pressures.

4.4 Further interpretation of measurements

To validate these measurements, one can analyze the slope of the gain curves for different pressures. Neglecting secondary effects (photon mediated effects, space charge and attachment), the gain G (electron multiplication) can be described using the first Townsend coefficient α [9]:

$$G = e^{\alpha d}$$

The thickness d of the multiplication zone is proportional to the number of THGEMs ($\#_{\text{THGEM}}$), since all THGEMs used have the same thickness. For low reduced electric

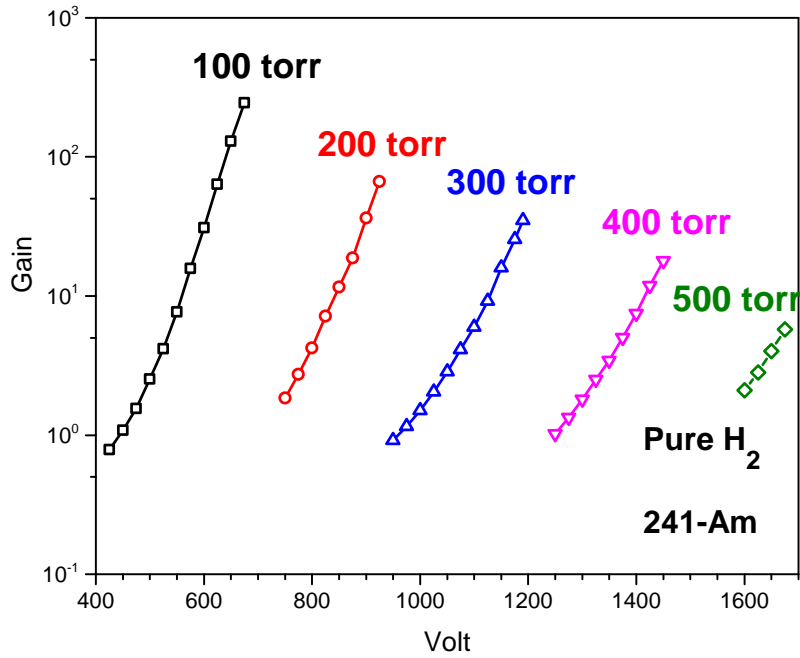


Figure 4.6: Comparison of the gain in pure hydrogen for different pressures. The curves in this graph are used to fit the parameter $\frac{\gamma}{p}$.

fields (smaller than 20 Volt/torr/cm), the first Townsend coefficient α is proportional to the

applied voltage V [7]. Therefore:

$$G = e^{\alpha d} \propto e^{V \#_{\text{THGEM}}}$$

Fitting all curves in Fig. 4.4 (Fig. 4.6) with $G \propto e^{\frac{\gamma}{p} V} \propto e^{V \#_{\text{THGEM}}}$ the parameter $\frac{\gamma}{p}$ only depends on the geometry of the configuration.

$$\frac{\gamma}{p} \propto \#_{\text{THGEM}}$$

Therefore plotting the results found in section 4 against the voltage instead of the reduced bias should lead to straight lines with the same inclination, since for $G = c \cdot e^{\frac{\gamma}{p} V}$ the logarithmic plot is $\log(G) = \log(c) + \log(e) \cdot \frac{\gamma}{p} V$ (Fig. 4.6). The values do not precisely match, making it clear that there is some error in the measurements or the assumptions, for the behavior of the gain are too simple. The results are presented in Tab. 4.2.

pressure	$\frac{\gamma}{p}$
100 torr	$0.0238 \frac{1}{\sqrt[3]{V}}$
200 torr	$0.0205 \frac{1}{\sqrt[3]{V}}$
300 torr	$0.0153 \frac{1}{\sqrt[3]{V}}$
400 torr	$0.0144 \frac{1}{\sqrt[3]{V}}$
500 torr	$0.0135 \frac{1}{\sqrt[3]{V}}$

Table 4.2: $\frac{\gamma}{p}$ calculated from the linear fits for the curves in Fig. 4.6.

Chapter 5

Towards a new generation of M-THGEMs: Three-layer M-THGEM

The three-layer M-THGEM was placed in the Prototype Active-Target Time Projection Chamber (pAT-TPC) [1] in order to investigate its performance. The pAT-TPC has a diameter of 28 cm, a length of 50 cm, and the same entrance window as the full size AT-TPC ($3.6\text{ }\mu\text{m}$ para-armid). The area covered by the M-THGEM has a diameter of 25 cm. Figure 5.1 shows a schematic drawings and a photograph of the M-THGEM electrode mounted on top of the pAT-TPC readout electronics. The same readout electronic and collimated

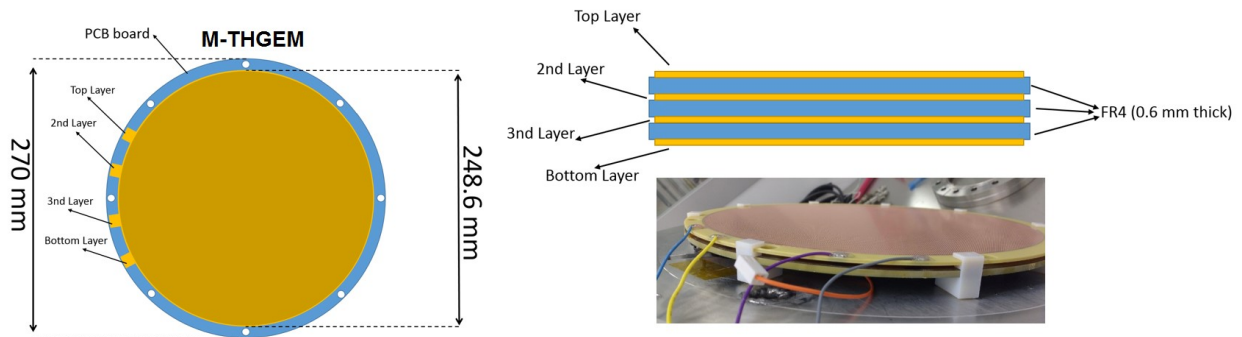


Figure 5.1: A schematic drawing (left (topview) and top right (sideview)) and a photograph (bottom right) of the mounted M-THGEM.

241-Am was used, as in the full size AT-TPC.

Figure 5.2 shows an example of an energy spectrum measured in He/(10%)CO₂ (black graph), compared to the expected spectrum computed by a Monte Carlo simulation us-

ing MCNPX (blue graph). The sharp peak corresponds to the energy released by particles emitted in the forward direction, which cross the whole active volume along the axis. The total energy deposited in the gas in this case is 2.4 MeV, with a measured energy dispersion of 5% (compared to the 4.5% computed with MCNPX simulations). The low-energy tail of the spectrum corresponds to alpha particles emitted at larger angles with respect to the cylindrical axis. These alpha particles exit the detector active volume and stop on the external walls of the field cage. The small differences between the computed and the simulated spectrum is most likely due to uncertainties when modeling the exact geometry of the collimator for the 241-Am source in MCNPX.

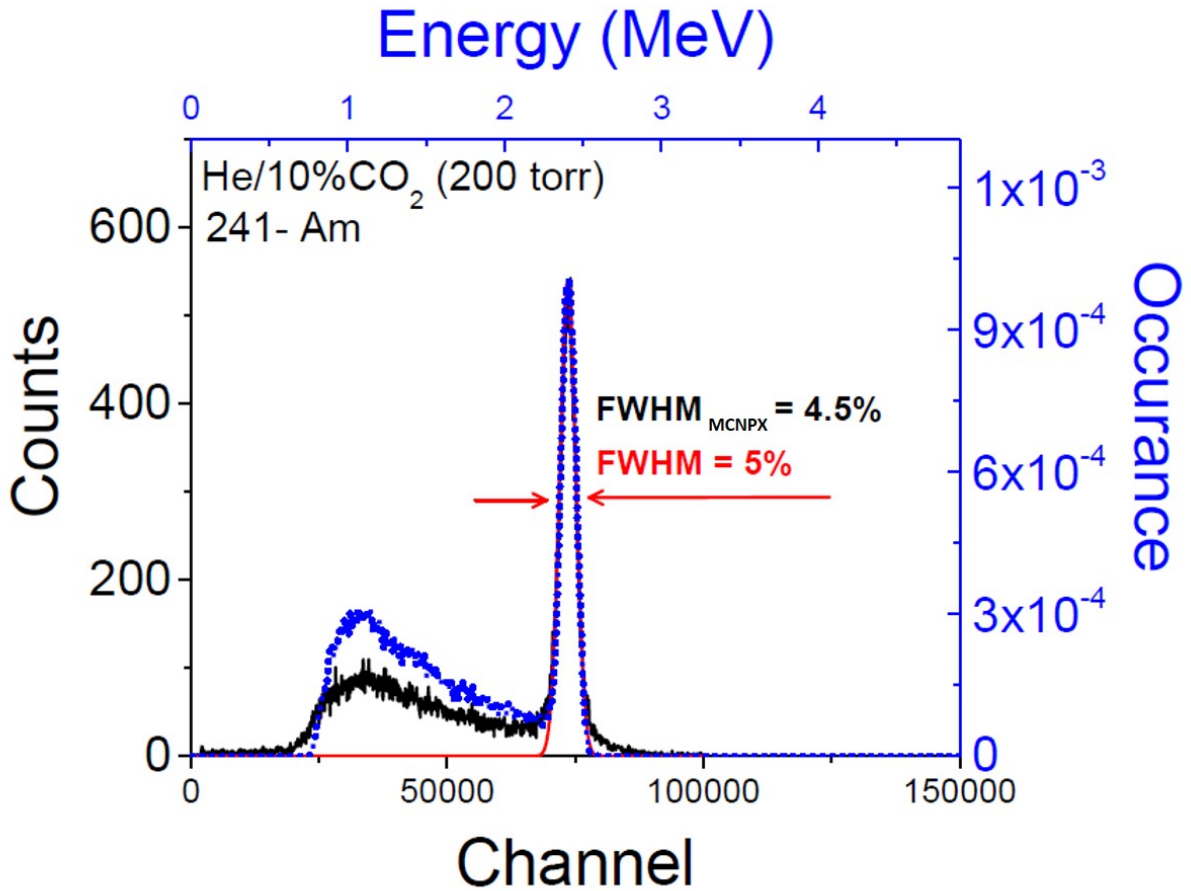


Figure 5.2: Spectrum of a 5.5 MeV alpha particle crossing the pAT-TPC active volume, recorded with the three layer M-THGEM operated in He-based mixture (10% CO₂).

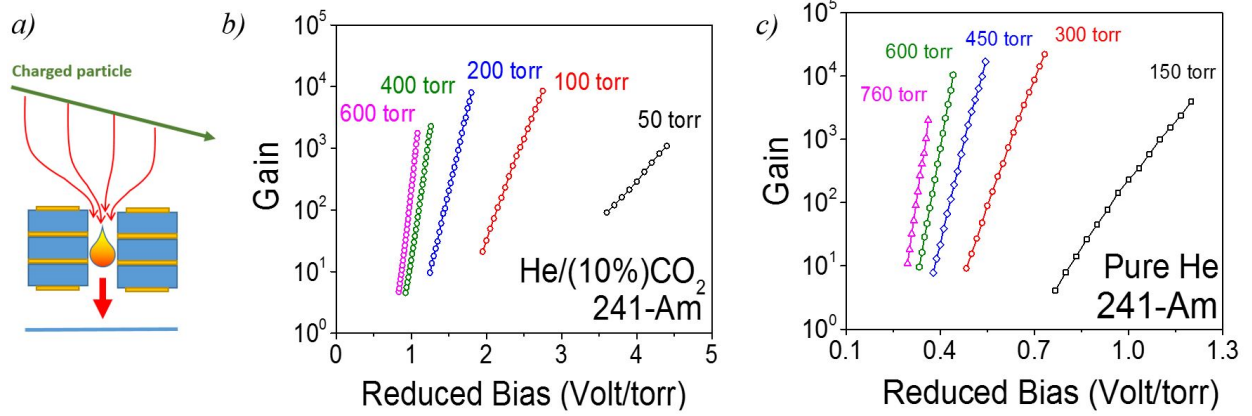


Figure 5.3: Gain measurement for the three layer M-THGEM (schematic drawing(a)) in He/(10%)CO₂ (b) and in pure He (c).

A maximum gain of $10^{4.5}$ was observed for both gases. The decrease of maximum achievable gain at high pressure is due to the smaller alpha particles range. This results in denser ionization (multiplication in a shorter time interval), therefore the maximum avalanche size is already reached at lower gain. Conversely, at very low pressure (below 100 torr) the detector shows large instabilities when relative high voltage is applied to the M-THGEM electrodes.

Operating the M-THGEM with a reduced voltage for the first stage has several advantages. The avalanche is squeezed towards the lower region of the M-THGEM, preventing photon-mediated effects from the top electrode surface. In addition, the first multiplier stage then acts as collector of positive charges, so that the ion backflow to the drift region is reduced. Using Maxwell the field map for a symmetrically biased (Fig. 5.4(a)) and an asymmetrically biased (reduced to $\approx 70\%$) (Fig. 5.4(b)) M-THGEM configuration were calculated. The gain curves of different asymmetric M-THGEM setups, measured in 200 torr He/10%CO₂ (Fig. 5.4(b)), shift towards higher reduced bias but reach the same maximum achievable gain. While full electron collection efficiency (Fig. 5.5(a)) is reached at a low hole-to-drift field ratio of 20 (corresponding to a gain of a few hundred), the asymmetric

setup shows a slightly better collection of ions in the first M-THGEM electrode, reducing the ion backflow. These results were simulated using Garfield [5], as described in section 3. A multi-cascade element is expected to reduce the IBF further, below 10%.

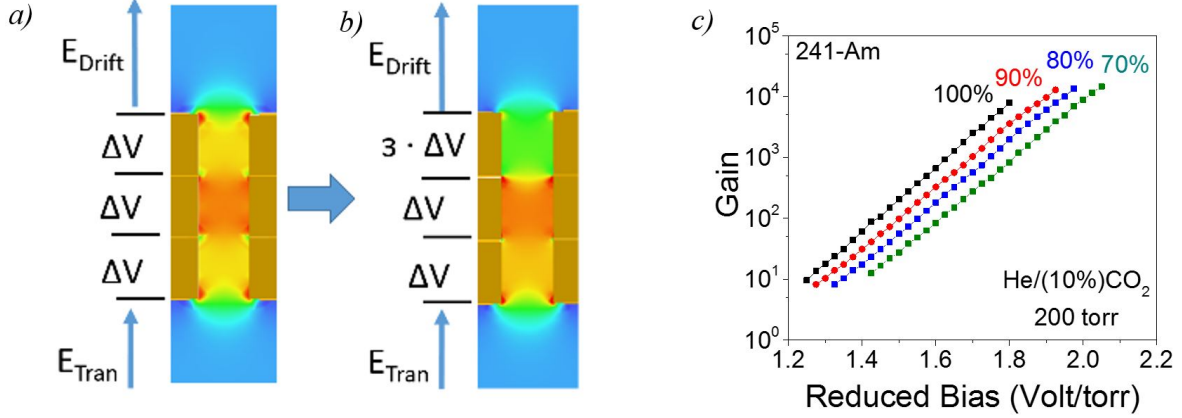


Figure 5.4: Comparison of the electric field map for a three layer M-THGEM hole symmetrically biased (a) and asymmetric biased (b). 3 represents the reduced fraction of the applied potential to the first multiplier stage. Measurements of effective gain in 200 torr $\text{He}/10\%\text{CO}_2$ for different three layer M-THGEM configurations.

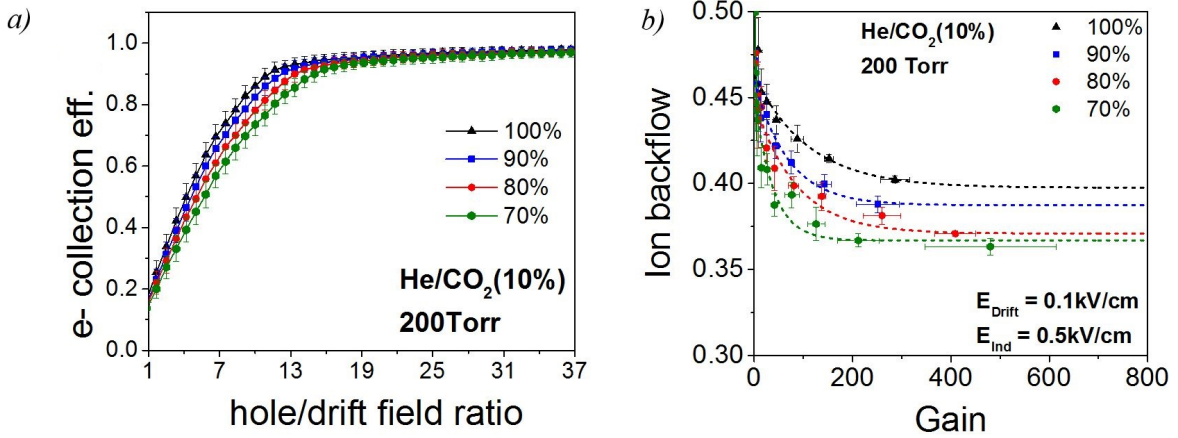


Figure 5.5: Comparison of the electron collection efficiency (a) and ion backflow (b) in $\text{He}/10\%\text{CO}_2$ for different asymmetric M-THGEM configurations.

Chapter 6

Conclusion and outlook

The THGEM is a hole-type gaseous electron multiplier produced by multi layer printed circuit board (PCB) technology. It consists of a densely perforated assembly of 0.6 mm thick FR-4 substrate, sandwiched between thin metallic electrode strata. Two Thick Gaseous Electron Multipliers (THGEM) in cascade were found to operate at a gain of up to 10^4 in pure helium for pressures between 200 torr and 600 torr, while also providing a good energy resolution. In pure hydrogen it was not possible to test the limit of the THGEM setup because the feedthrough in the AT-TPC was not designed for voltages above 1.5 kV and therefore limited the maximum voltage applied. Nevertheless a gain of $10^{2.5}$ was measured at a pressure of 100 torr.

Three THGEMs were sandwiched together to form a novel gaseous multiplier (M-THGEM), providing a high confinement of the electron avalanche within the hole, resulting in a gain of up to $10^{4.5}$ in pure low-pressure helium. Due to the geometric structure of the M-THGEM, the field is enhanced in the middle THGEM, confining the avalanche to that area. The three layer M-THGEM also showed a very good energy resolution of 5%, compared to the 4.5% computed with the MCNPX simulation. In Garfield [5], simulations of the ion backflow was found to be as low as 13% in certain conditions. Furthermore, this novel detector is extremely suitable to cover large areas due to its robustness and thickness of 1.8 mm. This makes the three layer M-THGEM a perfect device for the operation of a large AT-TPC.

In the near future the Penning effect should be included in the simulations, so that these

match the experimental results for pure helium. The AT-TPC should be equipped with a three layer M-THGEM to enable high gain in low pressure hydrogen and increase the energy resolution, as well as decrease the risk of failure due to the two THGEMs touching (mechanical bending). For further development of the M-THGEM it might be possible to use ceramic instead of FR-4, to reduce the charging up effect.

A future project could be to apply caesium iodide (CsI) to the top layer, which would emit electrons due to X-rays or photons. These electrons could then be multiplied in the M-THGEM. In that operation mode one would have to make sure that the ion backflow doesn't hit the top layer by choosing the appropriate field strength or geometry and possibly use a cascade setup.

APPENDICES

Appendix A

Additional graphs

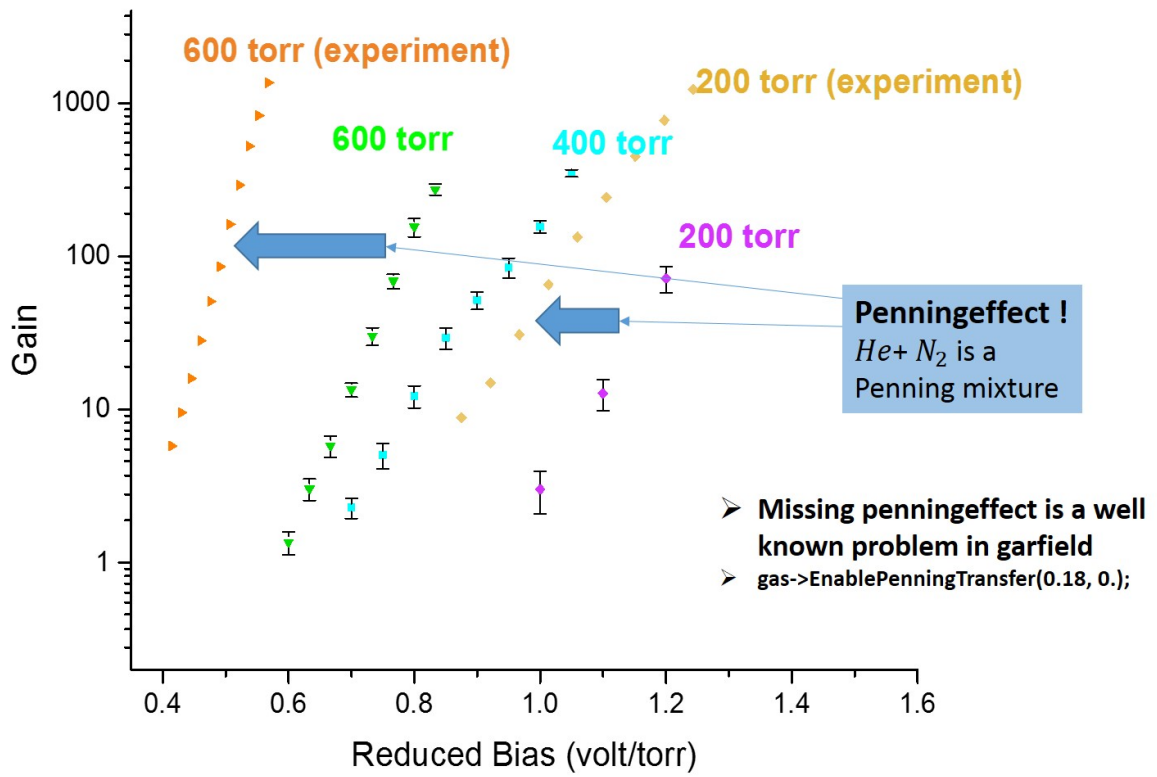


Figure A.1: Comparison between the experimental data (Fig. 4.2) in helium for the two cascade THGEMs and the simulated results (Fig. 3.9). The significant discrepancy can be explained by the missing Penning effect in garfield [5].

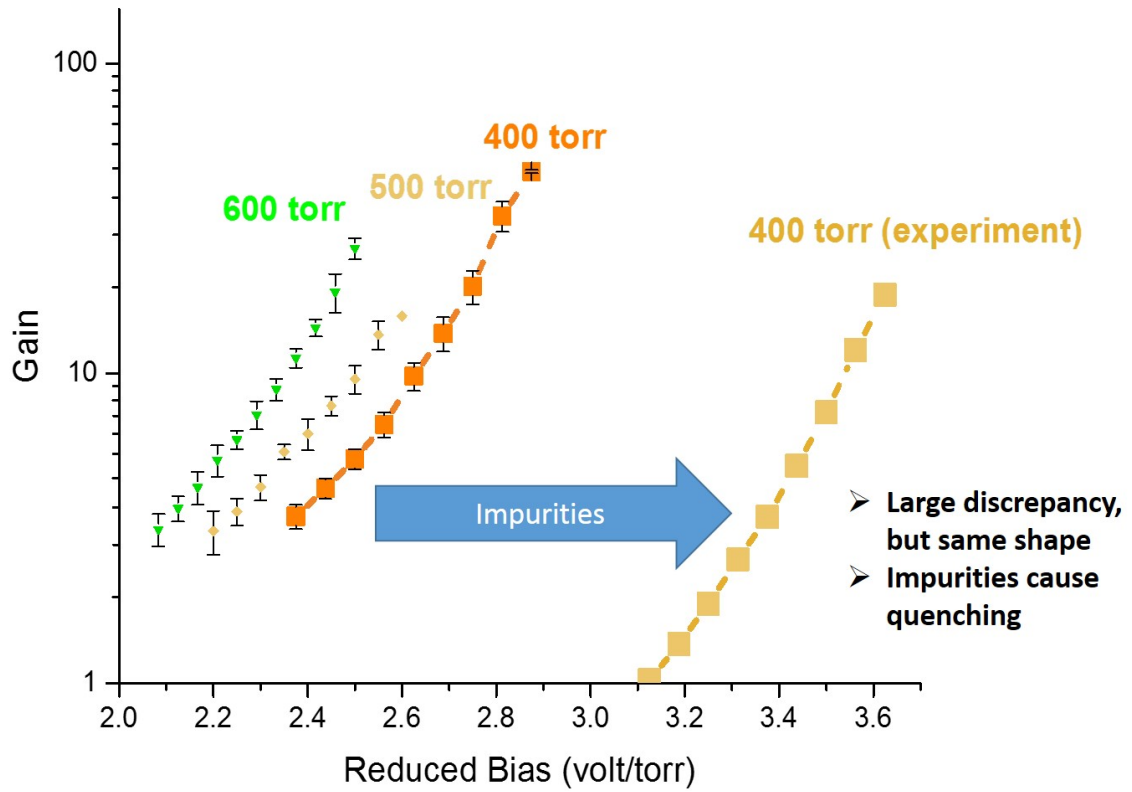


Figure A.2: Comparison between the experimental data (Fig. 4.4) in hydrogen for the two cascade THGEMs and the simulated results (Fig. 3.10). The significant discrepancy can be explained by residue oxygen, capturing free electrons.

Appendix B

Technical advice

The following is a list of technical tips in order to complete the experiment successfully:

- When screwing stainless steel screws in stainless steel NEVER use an automatic screw-driver! Best is when you even (if the place allows it) put some lubricant with the screw, to prevent it eating into the material
- Ground all measuring devices twice or even three times in order to reduce noise. Grounding cables can be used or even aluminium foil works well.
- When pumping (vacuum) be patient! It is best to pump below 500 mtorr (this is a lot less in actual gas pressure, because the system shows the pressures wrong in pure noble gases).
- The maximum pressure of the gas handling system is 700 torr. When you try to put more, an over pressure valve will open and you simply lose all your gas to the environment.
- Make sure to also vacuum all tubes before filling with gas, have detector chamber closed while doing so when you are doing it right before the operation due to leaks in the tube.

Appendix C

Manual for performing simulations of THGEMs within the NSCL

There is a demo folder stored in the group drive of Prof. Daniel Bazin, which makes the use of this manual easier, but it is not necessary.

C.1 Overview

Before the detailed description is given here a quick overview of what is happening. The aim is to automate simulations for many different gas pressures and voltages as far as possible and then run them in parallel on a batch system. The idea is to first create the necessary folders, then run ANSII Maxwell 11 and finally perform the simulation in Garfield using Magboltz.

Required software:

- Windows 7 (it is tested on windows 7 but should also run on other operation systems)
- Garfield 9 (this is installed on the fishtank and on the batch system (seaside))
- ANSII Maxwell 11 (not a newer version) the installation file is provided in the folder, and the license server for newer versions works fine
- MobaXterm_v8.6 or any other linux terminal (ssh)

- notepad++
- Origin 2016 or any other plotting software

Throughout the process it will be necessary to adapt the filenames and paths in each script, when doing so please be sure to include the correct “/” or “\” with it, depending on whether this specific part will be running in Linux or Windows. The suggestion is to use notepad++, since it is fast and efficient (multiple tabs).

C.2 Creating the folders and run files

Go to the folder:

I:\analysis\attpc\demofolder_simulation\triple_layer_voltage_30_h and run the file `create_all_voltages.bat`. This creates a folder for each voltage and copies the required files into it. It then runs a visualbasic script in order to perform the maxwell simulation. With the first loop the voltages are specified (“from”, “step”, “to”).

create_all_voltages.bat

```

1 setlocal enabledelayedexpansion
2 for /l %%n in (1000,25,1025) do (
3 mkdir %%nV_sym_auto
4 rmdir /S /Q thgem1.mxlresults
5 @rem new directory is created and old current directory in maxwell is deleted
6 @rem pause
7 @rem the VB script for maxwell is edited so that it runs the current voltage,
   this works by finding the entry 999 and replacing it
8 set txtfile=fullscript_2_edit.vbs
9 set newfile=fullscript_%%nV.vbs
10 if exist !newfile! del /f /q !newfile!
11 for /f "tokens=*" %%a in (!txtfile!) do (
12     set newline=%%a
13     set newline=!newline:^999=^%%n!
14     echo !newline! >> !newfile!
15 )
16 @rem pause
17 @rem required files are moved into the current folder

```

```

18 move fullscript_%%mV.vbs "I:\analysis\attpc\demofolder_simulation\
    triple_layer_voltage_30_h\%%nV_sym_auto\fullscript_%%mV.vbs"
19 copy copy_maxwell.bat "I:\analysis\attpc\demofolder_simulation\
    triple_layer_voltage_30_h\%%nV_sym_auto\*"
20 copy run "I:\analysis\attpc\demofolder_simulation\triple_layer_voltage_30_h\%%
    nV_sym_auto\*"
21 copy garftrans "I:\analysis\attpc\demofolder_simulation\
    triple_layer_voltage_30_h\%%nV_sym_auto\*"
22 @rem pause
23 @rem echo !volt!
24 @rem the VB script is run
25 cd I:\analysis\attpc\demofolder_simulation\triple_layer_voltage_30_h\%%
    nV_sym_auto
26 start /w fullscript_%%mV.vbs
27 cd I:\analysis\attpc\demofolder_simulation\triple_layer_voltage_30_h\%%
    nV_sym_auto
28 call copy_maxwell.bat
29 @rem all files neede for garfield are copied from maxwell
30 cd I:\analysis\attpc\demofolder_simulation\triple_layer_voltage_30_h
31 )
32 pause

```

The script takes the visual basic script (fullscript_2_edit.vbs) and replaces the voltage in it with the one specified in the loop.

C.3 Running Maxwell and creating file maps

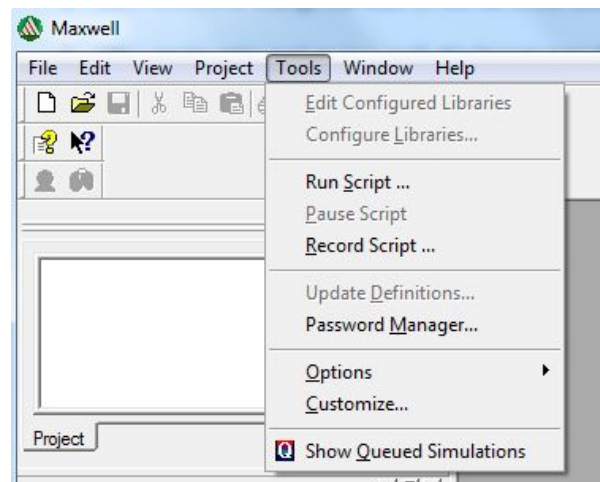


Figure C.1: “record script” function in Maxwell

The file fullscript_2_edit.vbs can be created in Maxwell by using the command

“record script” so that it gives flexibility to be used for different geometries and purposes. The script should include editing one or more global variables, which then appear in the visual basic (VB) script and can be edited by the `create_all_voltages.bat`. Therefore the variable to edit should be set to 999, so that the `create_all_voltages.bat` script can find it. Also the names of the maxwell file, folder path, and maxwell folder have to be up to date in the script and need to be changed when it is copied to a new folder (new set of simulations).

fullscript_2_edit.vbs

```

1  ' _____
2  ' Script Recorded by Maxwell Version 11.1.1
3  ' 10:02 PM Feb 08, 2016
4  ' _____
5  Dim oAnsoftApp
6  Dim oDesktop
7  Dim oProject
8  Dim oDesign
9  Dim oEditor
10 Dim oModule
11 Set oAnsoftApp = CreateObject("AnsoftMaxwell.MaxwellScriptInterface")
12 Set oDesktop = oAnsoftApp.GetAppDesktop()
13 oDesktop.RestoreWindow
14 oDesktop.OpenProject "I:/analysis/attpc/demofolder_simulation/
    triple_layer_voltage_30_h/thgem1.mxl"
15 Set oProject = oDesktop.SetActiveProject("thgem1")
16 Set oDesign = oProject.SetActiveDesign("MaxwellDesign1")
17 oProject.ChangeProperty Array("NAME: AllTabs", Array("NAME: ProjectVariableTab",
    Array("NAME: PropServers", -
18     "ProjectVariables"), Array("NAME: ChangedProps", Array("NAME: $voltagesym", "
    Value:=", "999"))))
19 oProject.Save
20 oDesign.AnalyzeAllNominal
21 Set oModule = oDesign.GetModule("FieldsReporter")
22 oModule.CalcStack "clear"
23 oModule.EnterQty "Voltage"
24 oModule.CalculatorWrite -
25     "I:\analysis\attpc\demofolder_simulation\triple_layer_voltage_30_h\999
    V.sym_auto\phi.reg", Array("Solution:=", -
26     "Setup1 : LastAdaptive"), Array("$voltagesym:=", "999", "a:=", "1mm", "d:=",
    -
27     "0.5mm", "h:=", "0.1mm", "t:=", "0.6mm")
28 oModule.CalcStack "clear"
29 oModule.EnterQty "E"
30 oModule.CalculatorWrite -
31     "I:\analysis\attpc\demofolder_simulation\triple_layer_voltage_30_h\999

```

```

32     V_sym_auto\e.reg", Array("Solution:=", -
    "Setup1 : LastAdaptive"), Array("$voltagesym:=", "999", "a:=", "1mm", "d:=",
33     -
    "0.5mm", "h:=", "0.1mm", "t:=", "0.6mm")
34 oModule.CalcStack "clear"
35 oModule.EnterQty "D"
36 oModule.CalculatorWrite -
37     "I:\analysis\attpc\demofolder_simulation\triple_layer_voltage_30_h\999
    V_sym_auto\d.reg", Array("Solution:=", -
38     "Setup1 : LastAdaptive"), Array("$voltagesym:=", "999", "a:=", "1mm", "d:=",
    -
39     "0.5mm", "h:=", "0.1mm", "t:=", "0.6mm")
40 oProject.Save
41 oDesktop.CloseProject "thgem1"

```

This script also saves the three field files needed from maxwell for garfield [5] (the potential, the electric field and the electric flux). In case it should be done manually, do the following: right click on field overlays -> calculator -> input -> quantities -> E-Field/D-Field/Voltage -> output -> write. These are also the steps to be followed when creating a new script. Once the VB script is finished `create_all_voltages.bat` runs the next script `copy_maxwell.bat` to copy the three field files from the maxwell folder (`fields.shd`, `current.hyd`, `current.pnt`) into the current voltage folder.

copy_maxwell.bat

```

1 echo Copy files starts:
2 echo f| xcopy /Y /S "I:\analysis\attpc\demofolder_simulation\
    triple_layer_voltage_30_h\thgem1.mxwresults\MaxwellDesign1.results\*
    current.hyd" current.hyd
3 echo f| xcopy "I:\analysis\attpc\demofolder_simulation\
    triple_layer_voltage_30_h\thgem1.mxwresults\MaxwellDesign1.results\*
    current.pnt" current.pnt /Y /S
4 echo f| xcopy "I:\analysis\attpc\demofolder_simulation\
    triple_layer_voltage_30_h\thgem1.mxwresults\MaxwellDesign1.results\*
    fields.shd" fields.shd /Y /S
5 @rem pause

```

Whenever the file name of the maxwell file is changed, the folder path changes and this then needs to be changed in `copy_maxwell.bat`.

Next `create_all_voltages.bat` copies the files required for garfield [5] into the current

voltage folder (`run`, `garftrans`).

`create_all_voltages.bat` finishes off with deleting the current maxwell working directory.

This is very important otherwise the field files fill up with more trash on every run. It will now start the next iteration of the “for” loop.

C.4 Run garfield on fishtank

Now that all the necessary files are in the folder, it is good to do a test run if everything works with visual output on fishtank before running hundreds of jobs on the seaside system.

Open `MobaXterm_Personal_8.6.exe` and start a new session, now select SSH and enter

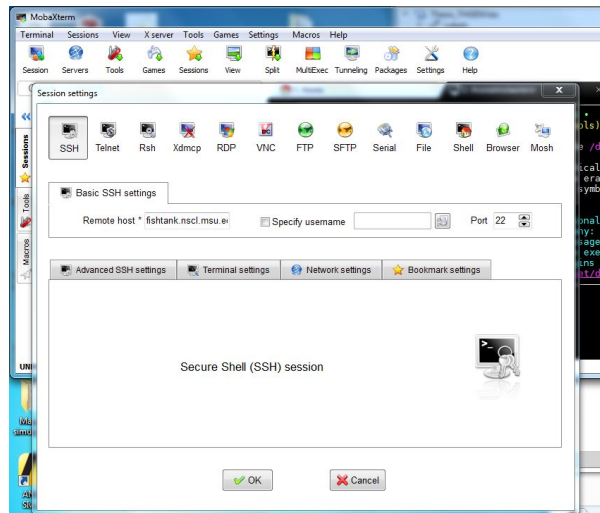


Figure C.2: Start Mobaxterm and enter host name.

the host name “fishtank.nsl.msu.edu”, click OK. Now login with your NSCL username and password. Go to the directory where you are working, if you work in the shared analysis drive where the demo folder is, you get there by entering:

```
1 cd /mnt/analysis/attpc/demofolder_simulation/triple_layer_voltage_30_h/
```


Now start garfield by entering:

```
1 module load garfield -9
2 garfield -9
3 1
4 < run
```

There is a file especially for running garfield with the graphic interface, the geometry information can be included at the designated position, so that the graphics output shows the THGEM.

run_view.txt

```
1 < garftrans
2 GLOBAL num = 1
3 GLOBAL pres_min = 100
4 GLOBAL pres_max = 700
5 GLOBAL pres_step = 100
6
7 //just assigned for loop precheck
8 Global bin 'temp.bin'
9     Global E_He_He =0
10    Global K_He_He =0
11 Global status =0
12 Global code =0
13
14 Vector pressures
15 400
16
17
18 For pres In pressures Do
19     For k From 1 Step 1 To num Do
20 !OPT NOGRID
21 !opt time-stamp
22 !opt linear-y
23 !rep labels          text-colour      black      text-font      higz
24 !rep numbers         text-colour      black      text-font      higz
25 !rep title           text-colour      black      text-font      higz
26 !rep comment         text-colour      black      text-font      higz
27 !rep message         text-colour      foreground text-font      higz
28 !layout x-number = 0.015, x-decade = 0.025, ...
29         y-number = 0.007, y-decade = 0.015, ...
30         x-label  = 0.010, y-label  = 0.010, ...
31         title    = 0.010
32 Global plotdrift True
33 Global d 'd.reg'
34 Global e 'e.reg'
35 Global phi 'phi.reg'
```

```

36 Global bin '3D-{pres}.bin '
37 Global exist false
38 &CELL
39 cell-id "Gain"
40 Call inquire_file(bin,exist)
41 If exist Then
42     read-field-map {bin}
43 Else
44     field-map files {phi} {e} {d} MAXWELL-11 ...
45     x-mirror-periodic y-mirror-periodic ...
46     plot-map
47 say "geometry created"
48     save-field-map {bin}
49 say "file saved"
50 Endif
51 solids
52 For x From -0.0866*4 Step 0.0866*2 To 0.0866*4 Do
53     For y From -0.05*4 Step 0.05*2 To 0.05*4 Do
54         hole centre {x,y} -0.03005 direction 0 0 1 ...
55         half-lengths 0.05 0.05 0.0005 ...
56         radius 0.035 ...
57         n = 5 ...
58         conductor-3
59         hole centre {x,y} +0.00 direction 0 0 1 ...
60         half-lengths 0.05 0.05 0.03 ...
61         radius 0.025 ...
62         n = 5 ...
63         dielectric
64         hole centre {x,y} +0.03005 direction 0 0 1 ...
65         half-lengths 0.05 0.05 0.0005 ...
66         radius 0.025 ...
67         n = 5 ...
68         conductor-3
69         hole centre {x,y} +0.0601 direction 0 0 1 ...
70         half-lengths 0.05 0.05 0.03 ...
71         radius 0.025 ...
72         n = 5 ...
73         dielectric
74         hole centre {x,y} +0.09015 direction 0 0 1 ...
75         half-lengths 0.05 0.05 0.0005 ...
76         radius 0.025 ...
77         n = 5 ...
78         conductor-3
79         hole centre {x,y} +0.1202 direction 0 0 1 ...
80         half-lengths 0.05 0.05 0.03 ...
81         radius 0.025 ...
82         n = 5 ...
83         dielectric
84         hole centre {x,y} +0.15025 direction 0 0 1 ...
85         half-lengths 0.05 0.05 0.0005 ...
86         radius 0.035 ...
87         n = 5 ...
88         conductor-3
89 Enddo

```



```

198 Global zd
199 Global nd
200 Global ewelll=0
201 Global multip
202 Global timep
203 Global ions=0
204 Global elect=0
205 Global conta=0
206
207 &DRIFT
208 area -0.2 -0.2 -0.2 0.2 0.2 0.5 CUT ...
209 view y=0 rotate 180.
210 *view -6*y+2*x+3*z=0 3D rotate -90.
211 integration-parameters m-c-dist-int 0.001
212 Call book_histogram(elec,50,0,2500)
213 Call book_histogram(ion,50,0,2500)
214 Call book_histogram(created,50,-0.02,+0.02)
215 Call book_histogram(lost,50,-0.02,+0.02)
216 Call book_histogram(end_e,50,-0.201,+0.501)
217 Call book_histogram(end_ion,50,-0.201,+0.501)
218 For i From 1 Step 1 To n Do
219     Global z=0.4
220     Global x=-0.0866+(RND_UNIFORM*2*0.0866)
221     Global y=-0.05+(RND_UNIFORM*2*0.05)
222
223     Call plot_drift_area
224     Call avalanche(x, y, z, 'plot-electron,plot-ion',ne,ni,...
225         'y_created',created,'y_lost',lost,'z_e',end_e,'z_ion',end_ion)
226     Call histogram_to_matrix(end_ion,a,min,max)
227     Call histogram_to_matrix(end_e,b,min,max)
228     Say "Electrons: {ne}, ions: {ni}, ion feedback: {a[50]}, electron feedback:
229         {b[1]}, fraction: {a[50]/b[1]}, gain: {b[1]/n} (avalanche {i})"
230     Call fill_histogram(elec,ne)
231     Call fill_histogram(ion,ni)
232     Global ions=ions+ni
233     Global elect=elect+ne
234     If (ne<1) Then
235         Global conta=conta+1
236     Endif
237 Enddo
238 *Call fit_exponential(elec,a,b,ea,eb,'plot')
239 *Say "Slope: {-1/b}"
240 *!options log-y
241 *Call plot_histogram(elec,'Electrons','Number of electrons after avalanche')
242 *Call plot_end
243 *Call hplot(ion,'Ions','Number of ions produced in avalanche')
244 *Call plot_end
245 *Call hplot(created,'y [cm]','Production point of electrons')
246 *Call plot_end
247 *Call hplot(lost,'y [cm]','Absorption point of electrons')
248 *Call plot_end
249 *Call hplot(end_e,'z [cm]','End point of electrons')
250 *Call plot_end
251 *Call hplot(end_ion,'z [cm]','End point of ions')

```

```

251 Call plot_end
252
253 > ionbackflow_{pres}.txt
254 Say "Electrons: {elect}, ions: {ions},ion feedback: {a[50]}, electron
    feedback: {b[1]},fraction:{a[50]/b[1]},gain:{b[1]/n}, number not detected
    = {conta}, total number= {n}, collection efficiency = {(n-conta)/n}, run={
    k}"
255 >
256 Enddo
257 Enddo
258 &MAIN

```

Hopefully all commenting within the file is clear and self explaining. For using a two cascade setup or a two cascade setup which is not aligned the following two geometries can be used. The only thing to keep in mind when creating geometries is that there is a limitation on the amount of “for loops” in garfield.

not_aligned_geometry.txt

```

1 solids
2 For x From -0.0866*4 Step 0.0866*2 To 0.0866*4 Do
3   For y From -0.05*4 Step 0.05*2 To 0.05*4 Do
4     hole centre {x,y} 0.0005 direction 0 0 1 ...
5     half-lengths 0.05 0.05 0.0005 ...
6     radius 0.035 ...
7     n = 5 ...
8     conductor-3
9     hole centre {x,y} +0.031 direction 0 0 1 ...
10    half-lengths 0.05 0.05 0.03 ...
11    radius 0.025 ...
12    n = 5 ...
13    dielectric
14    hole centre {x,y} +0.0615 direction 0 0 1 ...
15    half-lengths 0.05 0.05 0.0005 ...
16    radius 0.035 ...
17    n = 5 ...
18    conductor-3
19  Enddo
20  For y From -0.05*5 Step 0.05*2 To 0.05*5 Do
21    hole centre {x,y} +0.2625 direction 0 0 1 ...
22    half-lengths 0.05 0.05 0.0005 ...
23    radius 0.035 ...
24    n = 5 ...
25    conductor-3
26    hole centre {x,y} +0.293 direction 0 0 1 ...
27    half-lengths 0.05 0.05 0.03 ...
28    radius 0.025 ...
29    n = 5 ...
30    dielectric

```

```

31     hole centre {x,y} +0.3235 direction 0 0 1 ...
32     half-lengths 0.05 0.05 0.0005 ...
33     radius 0.035 ...
34     n = 5 ...
35     conductor-3
36 Enddo
37 Enddo
38 For x From -0.0866*5 Step 0.0866*2 To 0.0866*5 Do
39     For y From -0.05*5 Step 0.05*2 To 0.05*5 Do
40         hole centre {x,y} -0.0005 direction 0 0 1 ...
41         half-lengths 0.05 0.05 0.0005 ...
42         radius 0.035 ...
43         n = 5 ...
44         conductor-3
45         hole centre {x,y} +0.031 direction 0 0 1 ...
46         half-lengths 0.05 0.05 0.03 ...
47         radius 0.025 ...
48         n = 5 ...
49         dielectric
50         hole centre {x,y} +0.0615 direction 0 0 1 ...
51         half-lengths 0.05 0.05 0.0005 ...
52         radius 0.035 ...
53         n = 5 ...
54         conductor-3
55     Enddo
56     For y From -0.05*4 Step 0.05*2 To 0.05*4 Do
57         hole centre {x,y} +0.2625 direction 0 0 1 ...
58         half-lengths 0.05 0.05 0.0005 ...
59         radius 0.035 ...
60         n = 5 ...
61         conductor-3
62         hole centre {x,y} +0.293 direction 0 0 1 ...
63         half-lengths 0.05 0.05 0.03 ...
64         radius 0.025 ...
65         n = 5 ...
66         dielectric
67         hole centre {x,y} +0.3235 direction 0 0 1 ...
68         half-lengths 0.05 0.05 0.0005 ...
69         radius 0.035 ...
70         n = 5 ...
71         conductor-3
72     Enddo
73 Enddo

```

aligned_geometry.txt

```

1 solids
2 For x From -0.0866*4 Step 0.0866*2 To 0.0866*4 Do
3     For y From -0.05*4 Step 0.05*2 To 0.05*4 Do
4         hole centre {x,y} 0.0005 direction 0 0 1 ...
5         half-lengths 0.05 0.05 0.0005 ...
6         radius 0.035 ...
7         n = 5 ...

```

```

8         conductor-3
9     hole centre {x,y} +0.031 direction 0 0 1 ...
10         half-lengths 0.05 0.05 0.03 ...
11         radius 0.025 ...
12         n = 5 ...
13         dielectric
14     hole centre {x,y} +0.0615 direction 0 0 1 ...
15         half-lengths 0.05 0.05 0.0005 ...
16         radius 0.035 ...
17         n = 5 ...
18         conductor-3
19     hole centre {x,y} +0.2625 direction 0 0 1 ...
20         half-lengths 0.05 0.05 0.0005 ...
21         radius 0.035 ...
22         n = 5 ...
23         conductor-3
24     hole centre {x,y} +0.293 direction 0 0 1 ...
25         half-lengths 0.05 0.05 0.03 ...
26         radius 0.025 ...
27         n = 5 ...
28         dielectric
29     hole centre {x,y} +0.3235 direction 0 0 1 ...
30         half-lengths 0.05 0.05 0.0005 ...
31         radius 0.035 ...
32         n = 5 ...
33         conductor-3
34 Enddo
35 Enddo
36 For x From -0.0866*5 Step 0.0866*2 To 0.0866*5 Do
37     For y From -0.05*5 Step 0.05*2 To 0.05*5 Do
38         hole centre {x,y} -0.0005 direction 0 0 1 ...
39         half-lengths 0.05 0.05 0.0005 ...
40         radius 0.035 ...
41         n = 5 ...
42         conductor-3
43     hole centre {x,y} +0.031 direction 0 0 1 ...
44         half-lengths 0.05 0.05 0.03 ...
45         radius 0.025 ...
46         n = 5 ...
47         dielectric
48     hole centre {x,y} +0.0615 direction 0 0 1 ...
49         half-lengths 0.05 0.05 0.0005 ...
50         radius 0.035 ...
51         n = 5 ...
52         conductor-3
53     hole centre {x,y} +0.2625 direction 0 0 1 ...
54         half-lengths 0.05 0.05 0.0005 ...
55         radius 0.035 ...
56         n = 5 ...
57         conductor-3
58     hole centre {x,y} +0.293 direction 0 0 1 ...
59         half-lengths 0.05 0.05 0.03 ...
60         radius 0.025 ...
61         n = 5 ...

```



```

62         dielectric
63     hole centre {x,y} +0.3235 direction 0 0 1 ...
64         half-lengths 0.05 0.05 0.0005 ...
65         radius 0.035 ...
66         n = 5 ...
67         conductor -3
68     Enddo
69 Enddo

```

C.5 Run garfield on the seaside batch system - create job files

To run many different voltages at the same time the seaside batch system can be used. To use it each separat job must have its own job file, these are created with `create_job_files.bat` and can then be submitted as one single file.

create_job_files.bat

```

1 setlocal enabledelayedexpansion
2 for /l %%n in (1000,25,1025) do (
3     set txtfile=job_standard.sh
4     set newfile=job.sh
5     if exist !newfile! del /f /q !newfile!
6     for /f "tokens=*" %%a in (!txtfile!) do (
7         set newline=%%a
8         set newline=!newline:~999=^%%~n!
9         echo !newline! >> !newfile!
10    )
11    @rem replacing all the 999 in the job file with the current voltage and then
12    copying it
13    move job.sh "I:\analysis\attpc\demofolder_simulation\triple_layer_voltage_30_h\
14    \%%~nV_sym_auto\job.sh"
15    copy run "I:\analysis\attpc\demofolder_simulation\triple_layer_voltage_30_h\%%~nV_sym_auto\*"
16    @rem copying the run file in case it changed
17    cd I:\analysis\attpc\demofolder_simulation\
18    @rem creating the file which will be submitted
19    echo cd /mnt/analysis/attpc/demofolder_simulation/triple_layer_voltage_30_h/%%~nV_sym_auto/ >>submit.sh
20    echo qsub /mnt/analysis/attpc/demofolder_simulation/triple_layer_voltage_30_h/
21    /%%~nV_sym_auto/job.sh >>submit.sh
22    cd I:\analysis\attpc\demofolder_simulation\triple_layer_voltage_30_h\
23    )

```

`create_job_files.bat` edits the `job_standard.sh` file for each voltage and copies it then into the specific folder. For this file also the filenames and folder paths as well as the voltages need to be changed and match with all other scripts.

job_standard.sh

```
1 # pbs template script
2
3
4 #### Set the job name
5
6 ##PBS -N Target
7
8
9 #### Have PBS mail you results
10
11 #PBS -M rost@nscl.msu.edu
12
13
14 # Email generated at beginning, abort, and end of jobs
15
16 #PBS -m bae
17
18 #PBS -l nodes=1
19
20 #PBS -l walltime=72:00:00
21
22
23 #### Combine stdout/stderr
24
25 #### Note, this output directory must exist, or job will fail with:
26
27 ####   Aborted by PBS Server
28
29 ####   Job cannot be executed
30
31 #### Also, don't use "~" in path, also seems to fail.
32
33 #PBS -j oe
34
35 #PBS -o $PBS_JOBID.$PBS_JOBNAME.out
36
37
38 module load garfield -9
39
40
41 # go to where qsub was run from
42 cd $PBS_O_WORKDIR
43
44
45 # or maybe
```

```

46
47 # cd /mnt/analysis/attpc/Rost/..
48
49 printenv
50
51
52
53
54
55 cd /mnt/analysis/attpc/demofolder_simulation/triple_layer_voltage_30_h/999
    V_sym_auto/ #changes folder path in linux
56 # the | in the next line is vital because it passes on the run file so that it
    read line by line
57 cat run | garfield-9

```

For each of these files an entry is made in the final file for submission to the seaside system.

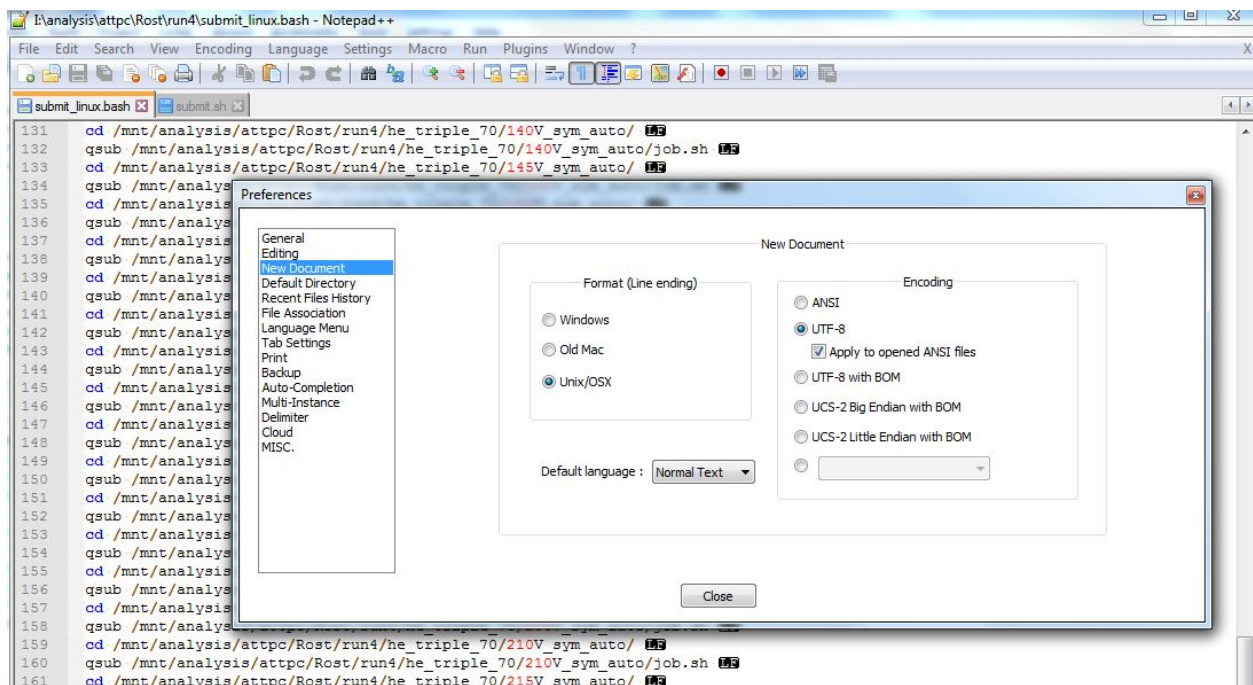
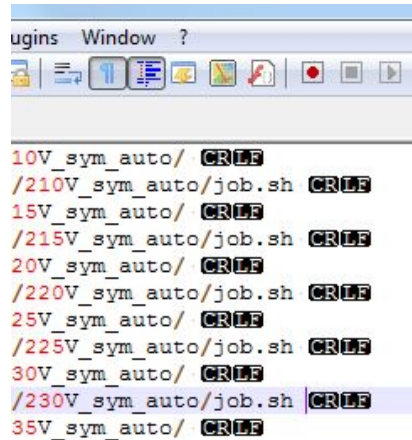


Figure C.3: Correct settings in notepad++, to modify the file for submitting to the batch system. The correct line ending “LF” is shown.

`submit.sh` can not be submitted to the seaside system. The linebreak has to be changed from windows to linux format. This step is crucial and can not be skipped. Configure notepad in its setting so that it looks like Fig. C.3. Basically change the line ending setting to linux and enable that line endings are displayed. Now create a new file (`submit_linux.sh`)



```
ugins Window ?
10V_sym_auto/ CR LF
/210V_sym_auto/job.sh CR LF
15V_sym_auto/ CR LF
/215V_sym_auto/job.sh CR LF
20V_sym_auto/ CR LF
/220V_sym_auto/job.sh CR LF
25V_sym_auto/ CR LF
/225V_sym_auto/job.sh CR LF
30V_sym_auto/ CR LF
/230V_sym_auto/job.sh CR LF
35V_sym_auto/ CR LF
```

Figure C.4: Wrong (windows) line break in the file for submitting to the batch system.

and copy all the content from `submit.sh` into the new file. It should now only say “LF” at the line ending, like in Fig. C.3, not “CR LF” like in Fig. C.4.

Log onto the seaside system:

open `MobaXterm_Personal_8.6.exe` and start a new session, now select SSH and enter the host name “seaside.nscl.msu.edu”, click OK. Now login with your NSCL username and password. Go to the directory where `submit_linux.sh` is located. If you work in the shared analysis drive where the demo folder is, you get there by entering:

```
1 cd /mnt/analysis/attpc/demofolder_simulation/
```

Now simply type

```
1 submit_linux.sh
```

and press enter. A whole bunch of jobs will be submitted, you can view your current status with

```
1 qstat -a
```

a job can be deleted with

```
1 qdel [job ID]
```

Hint: If you have to delete many jobs, do an excel sheet and copy paste it into the terminal (with right click).

C.6 Extracting the data with Matlab

result_ion_transport.m

```
1 clear all;
2 close all;
3 addpath('H:\My Documents\Matlab_scripts\matlabfrag') %not needed unless
   using mlf2pdf script (not needed)
4 save='symmetric_voltage_field_500V_per_cm'; %not particularly important can
   be changed later when saving
5 pfad = 'I:\analysis\attpc\demofolder_simulation\triple_layer_voltage_30_h';
   %filepath -> has to be changed
6 gas_step=200; %definition of steps for gas and voltages
7 gas_start=200;
8 gas_finish=600;
9 voltage_start=300;
10 voltage_finish=1300;
11 voltage_step=25;
12 gas_p = gas_start:gas_step:gas_finish; %definition o vectors needed when
   reading files
13 voltage=voltage_start:voltage_step:voltage_finish;
14 multi_r=zeros(size(voltage,2),size(gas_p,2));
15 effi_r=zeros(size(voltage,2),size(gas_p,2));
16 for i_voltage = 1:size(voltage,2); %reading files (votlages)
17     str_voltage=num2str(voltage(i_voltage));
18     full_pfad=[pfad '\ ' str_voltage 'V_sym_auto']; %creating fielpath
   within loop -> edit when file name changes
19     for i_gas_p = 1:size(gas_p,2);
20         if gas_p(i_gas_p)==750
21             gas_p(i_gas_p)=760;
22         end
23         str_gas = num2str(gas_p(i_gas_p));
24         name = [full_pfad '\ionbackflow_' str_gas '.txt'];
25         if exist(name, 'file') %reading of files which exist
26             k=0;
27             m=0;
28             fid = fopen(name);
29             tline=fgetl(fid);
30             % tline=fgetl(fid); %this line can be deleted
31             while ischar(tline)
32                 % for i=1:200;
33                 k=k+1;
34                 char_array(k)=textscan(tline, '%s', 'Delimiter', '\t,:');
35                 for p=1:size(char_array{k},1)
36                     temp_char_str_m=char_array{k}{p};
```

```

37         test='fraction';
38         if strcmp(temp_char_str_m, test)
39             m=m+1;
40             multi_r(i_voltage, i_gas_p, m)=str2num(char_array{k}{p
+3});
41             effi_r(i_voltage, i_gas_p, m)=str2num(char_array{k}{p
+1});
42         end
43     end
44     tline=fgetl(fid);
45 end
46 fclose(fid);
47 end
48 if mod(i_gas_p, 2) ==0
49     Progress=i_gas_p/size(gas_p, 2)      %this progress loop is not
complete but gives an idea that the file is running
50 end
51 end
52 end
53 display('————reading of data completed————')
54 %%
55 for g1=1:1:size(multi_r, 2);      %calculating all the mean values and standard
diviation for the runs
56     for v1=1:1:size(multi_r, 1);
57         temp_multi_full=multi_r(v1, g1, :);
58         temp_effi_full=effi_r(v1, g1, :);
59         temp_effi=temp_effi_full(temp_effi_full~=0);
60         temp_multi=temp_multi_full(temp_multi_full~=0);
61         multi_std(v1, g1)=std(temp_multi, 1, 3);
62         effi_std(v1, g1)=std(temp_effi, 1, 3);
63         multi_mean(v1, g1)=mean(temp_multi, 3);
64         effi_mean(v1, g1)=mean(temp_effi, 3);
65     end
66 end
67 effi_mean(isnan(effi_mean))=0;      %making sure there are no "empty fields"
68 effi_std(isnan(effi_std))=0;
69 multi_mean(isnan(multi_mean))=0;
70 multi_std(isnan(multi_std))=0;
71 % multi_std=std(multi_r, 1, 3);
72 % effi_std=std( effi_r, 1, 3);
73 % multi_mean=mean(multi_r, 3);
74 % effi_mean=mean( effi_r, 3);
75 %%
76 max_multi=5E6;      %cut off for data -> edit as needed
77 start_cutoff=1;
78 plot_step=200;
79 plot_start=gas_start;      %output selection
80 plot_finish=gas_finish;
81 graph_number=0;
82 for gas_evl=plot_start:plot_step:plot_finish;
83     % gas_evl=150;
84     gas_position=(gas_evl-gas_start)/gas_step+1;
85     cutoff=0;
86     start=1;

```

```

87 voltage_number=0;
88 for t1=1:size(voltage,2)
89     if multi_mean(t1,gas_position)<max_multi
90         if multi_mean(t1,gas_position)>start_cutoff
91             voltage_number=voltage_number+1;
92             plot_multi(voltage_number,1)=voltage(t1);
93             plot_multi(voltage_number,2)=multi_mean(t1,gas_position);
94             plot_multi(voltage_number,3)=multi_std(t1,gas_position);
95
96             plot_effi(voltage_number,1)=voltage(t1);
97             plot_effi(voltage_number,2)=effi_mean(t1,gas_position);
98             plot_effi(voltage_number,3)=effi_std(t1,gas_position);
99         end
100     end
101 end
102 if exist('plot_effi'); %plotting and saving
103     graph_number=graph_number+1;
104     color=rand(1,3);
105     if gas_evl==750
106         gas_evl=760;
107     end
108     figure(1)
109     errorbar(plot_effi(:,1),plot_effi(:,2),plot_effi(:,3), '-*', 'color',
color)
110     grid on;
111     hold on;
112     legd1{graph_number}=['gas pressure: ' num2str(gas_evl) 'torr'];
113     xlabel 'voltage [V]';
114     ylabel 'ion feedback I_a/I_c';
115     fig1=gcf;
116     % mlf2pdf(1,['multiplication ' num2str(gas_evl)]);
117
118     figure(2)
119     errorbar(plot_multi(:,1),plot_multi(:,2),plot_multi(:,3)*3, '-*', '
color',color)
120     set(gca,'yscale','log')
121     grid on;
122     hold on;
123     legd2{graph_number}=['gas pressure: ' num2str(gas_evl) 'torr'];
124     xlabel 'voltage [V]';
125     ylabel 'multiplication';
126     fig2=gcf;
127     csvwrite(['final_multi ' num2str(gas_evl) 'torr.csv'],plot_multi); %
saving as csv data
128     csvwrite(['final_ion ' num2str(gas_evl) 'torr.csv'],plot_effi);
129     % mlf2pdf(1,['efficiency ' num2str(gas_evl)]);
130 end
131 clear plot_effi plot_multi %neededso that no size error occure for the
next pressure
132 end
133 figure(1)
134 legend(legd1,'Location','southeast')
135 hold off

```

```
137 figure(2)
138 legend(legd2, 'Location', 'eastoutside')
139 hold off
140 clear legd1 legd2 graph_number %neede to create a new title and legend next
    run
```

After extracting the data into spreadsheets, it can be plotted with any good plotting software, for example Origin.

C.7 Summary

1. Prepare all files by updating the folder path and file names
2. run `create_all_voltages.bat`
3. run `create_job_files.bat`
4. edit the line break in `submit.sh`
5. log on to `seaside.nsl.msu.edu` and submit `submit_linux.sh`

BIBLIOGRAPHY

BIBLIOGRAPHY

- [1] D. Suzuki, M. Ford, D. Bazin, W. Mittig, W.G. Lynch, T. Ahn, S. Aune, E. Galyaev, A. Fritsch, J. Gilbert, F. Montes, A. Shore, J. Yurkon, J.J. Kolata, J. Browne, A. Howard, A.L. Roberts, and X.D. Tang. Prototype AT-TPC: Toward a new generation active target time projection chamber for radioactive beam experiments. *Nuclear Instruments and Methods in Physics Research Section A: Accelerators, Spectrometers, Detectors and Associated Equipment*, 691:39–54, November 2012.
- [2] National superconducting cyclotron laboratory, michigan state university, east lansing, mi 48824, usa.
- [3] M.S. Wallace, M.A. Famiano, M.-J. van Goethem, A.M. Rogers, W.G. Lynch, J. Clifford, F. Delaunay, J. Lee, S. Labostov, M. Mocko, L. Morris, A. Moroni, B.E. Nett, D.J. Oostdyk, R. Krishnasamy, M.B. Tsang, R.T. de Souza, S. Hudan, L.G. Sobotka, R.J. Charity, J. Elson, and G.L. Engel. The high resolution array (HiRA) for rare isotope beam experiments. *Nuclear Instruments and Methods in Physics Research Section A: Accelerators, Spectrometers, Detectors and Associated Equipment*, 583(2-3):302–312, December 2007.
- [4] A.H. Wuosmaa, J.P. Schiffer, B.B. Back, C.J. Lister, and K.E. Rehm. A solenoidal spectrometer for reactions in inverse kinematics. *Nuclear Instruments and Methods in Physics Research Section A: Accelerators, Spectrometers, Detectors and Associated Equipment*, 580(3):1290–1300, October 2007.
- [5] R. Veenhof. Garfield, a drift chamber simulation program. 1998.
- [6] Yu I. Davydov. On the first Townsend coefficient at high electric field. *arXiv preprint physics/0409156*, 2004.
- [7] Lorne M. Chanin and G. D. Rork. Experimental determinations of the first Townsend ionization coefficient in helium. *Physical Review*, 133(4A):1005, 1964.
- [8] B. Azmoun, W. Anderson, D. Crary, J. Durham, T. Hemmick, J. Kamin, G. Karagiorgi, K. Kearney, G. Keeler, E. Kornacki, and others. A study of gain stability and charging effects in GEM foils. In *Nuclear Science Symposium Conference Record, 2006. IEEE*, volume 6, pages 3847–3851. IEEE, 2006.

- [9] M. Cortesi, J. Yurkon, and A. Stolz. Operation of a THGEM-based detector in low-pressure Helium. *Journal of Instrumentation*, 10(02):P02012, 2015.
- [10] Th. G Schut and J. A Smit. A direct measurement of the efficiency of the penning-effect. *Physica*, 10(6):440–444, June 1943.
- [11] Fabio Sauli. *Gaseous radiation detectors: fundamentals and applications*. Cambridge monographs on particle physics, nuclear physics and cosmology. Cambridge Univ. Press, Cambridge, 2014.
- [12] Fabio Sauli. *Principles of operation of multiwire proportional and drift chambers*. Lectures given in the academic training programm of CERN 1975-1979. CERN - Service d’Information scientifique - RD/233, Geneva, 1977.
- [13] Fabio Sauli. *Gaseous radiation detectors: fundamentals and applications*. Cambridge monographs on particle physics, nuclear physics and cosmology. Cambridge Univ. Press, Cambridge, 2014.
- [14] M. Cortesi, V. Peskov, G. Bartesaghi, J. Miyamoto, S. Cohen, R. Chechik, J. M. Maia, J. M. F. dos Santos, G. Gambarini, V. Dangendorf, and others. THGEM operation in Ne and Ne/CH₄. *Journal of Instrumentation*, 4(08):P08001, 2009.
- [15] O. Bouianov, M. Bouianov, R. Orava, P. Semenov, and V. Tikhonov. Progress in GEM simulation. *Nuclear Instruments and Methods in Physics Research Section A: Accelerators, Spectrometers, Detectors and Associated Equipment*, 450(2):277–287, 2000.
- [16] Ansoft Corporation. Ansoft maxwell 3d field simulator, version 11. *Four Station Square Suite 200 Pittsburgh, PA 15219, USA*.
- [17] OAK RIDGE NATIONAL LABORATORY. Mcnpx 2.4.0. *Los Alamos National Laboratory, Los Alamos, New Mexico*.
- [18] H. W. Ellis, R. Y. Pai, E. W. McDaniel, E. A. Mason, and L. A. Viehland. Transport properties of gaseous ions over a wide energy range. *Atomic Data and Nuclear Data Tables*, 17(3):177–210, March 1976.
- [19] H. W. Ellis, E. W. McDaniel, D. L. Albritton, L. A. Viehland, S. L. Lin, and E. A. Mason. Transport properties of gaseous ions over a wide energy range. Part II. *Atomic Data and Nuclear Data Tables*, 22(3):179–217, September 1978.
- [20] Bin-Long Wang, Qian Liu, Hong-Bang Liu, Xiao-Kang Zhou, Shi Chen, Dong-Sheng Ge, Wen-Qian Huang, Yi-Gang Xie, Yang-Heng Zheng, Yang Dong, Qiang Zhang, Xin-

Da Jiao, Jing Wang, Min Li, and Jie Chang. Ion Transportation Study for Thick Gas Electron Multipliers. *Chinese Physics Letters*, 31(12):122901, December 2014.

- [21] France Laboratoire de Physique Corpusculaire de Caen. Faster project. *website:* <http://faster.in2p3.fr/>.
- [22] Simon Wedlund et al. Comprehensive calculation of the energy per ion pair or w values for five major planetary upper atmospheres. *Annales Geophysicae*, 29(1):187–195, January 2011.